



Early View

Original research article

***Lrig1* expression identifies airway basal cells with high proliferative capacity and restricts lung squamous cell carcinoma growth**

Laura Sucony, Sandra Gómez-López, Adam Pennycuick, Ahmed S. N. Alhendi, Derek Davies, Sarah E. Clarke, Kate H.C. Gowers, Nicholas A. Wright, Kim B. Jensen, Sam M. Janes

Please cite this article as: Sucony L, Gómez-López S, Pennycuick A, *et al.* *Lrig1* expression identifies airway basal cells with high proliferative capacity and restricts lung squamous cell carcinoma growth. *Eur Respir J* 2021; in press (<https://doi.org/10.1183/13993003.00816-2020>).

This manuscript has recently been accepted for publication in the *European Respiratory Journal*. It is published here in its accepted form prior to copyediting and typesetting by our production team. After these production processes are complete and the authors have approved the resulting proofs, the article will move to the latest issue of the ERJ online.

Copyright ©The authors 2021. This version is distributed under the terms of the Creative Commons Attribution Licence 4.0.

***Lrig1* expression identifies airway basal cells with high proliferative capacity
and restricts lung squamous cell carcinoma growth**

Laura Sucony^{1,5}, Sandra Gómez-López^{1,5}, Adam Pennycuick¹, Ahmed S. N. Alhendí¹, Derek Davies², Sarah E. Clarke¹, Kate H.C. Gowers¹, Nicholas A. Wright³, Kim B. Jensen⁴, Sam M. Janes¹

¹ Lungs for Living Research Centre, UCL Respiratory, University College London, London, UK

² Flow Cytometry Facility, Francis Crick Institute, London, UK

³ Centre for Tumour Biology, Barts Cancer Institute, Queen Mary University of London, London, UK

⁴ Biotech Research and Innovation Centre, University of Copenhagen; Novo Nordisk Foundation Center for Stem Cell Biology, DanStem, University of Copenhagen, Denmark

⁵ These authors contributed equally to this work

Corresponding author: Sam M. Janes

Address: Lungs for Living Research Centre, UCL Respiratory, University College London, 5 University Street, London, WC1E 6JF, UK

Phone: (+44) 020 3549 5979

E-mail: s.janes@ucl.ac.uk

Take home message:

LRIG1 is lost in development of squamous cell lung cancers. We show LRIG1 marks basal airway progenitor cells with high proliferative potential and regulates progression of pre-invasive squamous cell lung cancer.

ABSTRACT

Lung squamous cell carcinoma (LUSC) accounts for a significant proportion of cancer deaths worldwide, and is preceded by the appearance of progressively disorganised pre-invasive lesions in the airway epithelium. Yet the biological mechanisms underlying progression of pre-invasive lesions into invasive LUSC are not fully understood. *LRIG1* is downregulated in pre-invasive airway lesions and invasive LUSC tumours and this correlates with decreased lung cancer patient survival.

Using an *Lrig1* knock-in reporter mouse and human airway epithelial cells collected at bronchoscopy, we show that during homeostasis LRIG1 is heterogeneously expressed in the airway epithelium. In basal airway epithelial cells, the suspected cell of origin of LUSC, LRIG1 identifies a subpopulation of progenitor cells with higher *in vitro* proliferative and self-renewal potential in both the mouse and human. Using the N-nitroso-tris-chloroethylurea (NTCU)-induced murine model of LUSC, we find that *Lrig1* loss-of-function leads to abnormally high cell proliferation during the earliest stages of pre-invasive disease and to the formation of significantly larger invasive tumours, suggesting accelerated disease progression.

Together, our findings identify LRIG1 as a marker of basal airway progenitor cells with high proliferative potential and as a regulator of pre-invasive lung cancer progression. This work highlights the clinical relevance of LRIG1 and the potential of the NTCU-induced LUSC model for functional assessment of candidate tumour suppressors and oncogenes.

INTRODUCTION

Lung cancer is the main cause of cancer-related deaths worldwide with 2.1 million new cases diagnosed each year [1]. The majority of patients present with late-stage incurable disease [2], therefore devising strategies for early detection and treatment is key to improving lung cancer outcomes.

85% of lung cancer cases are non-small-cell lung cancer (NSCLC), of which a third are lung squamous cell carcinoma (LUSC) [3, 4]. LUSC arises in the bronchial epithelium, preceded by the development of progressively disordered pre-invasive lesions, ranging from metaplasia to increasing grades of dysplasia and carcinoma *in situ* (CIS) [5, 6]. Pre-invasive squamous airway lesions are associated with tobacco cigarette smoking, the predominant lung cancer risk factor [5, 7, 8]. Molecular studies have identified genetic, epigenetic and transcriptional changes in pre-invasive lesions [9-13]. However, the biological relevance of these changes in lung cancer development is not understood.

Leucine rich repeats and immunoglobulin like domains 1 (LRIG1) is a transmembrane protein that acts as a negative regulator of epidermal growth factor receptor (EGFR) signalling [14, 15]. *LRIG1* is located in chromosome 3p14, a region that is frequently affected by copy number alterations in pre-invasive lung lesions and NSCLC [16, 17]. Loss of heterozygosity (LOH) of *LRIG1* is seen in 75% of human lung cancer cell lines and low levels of *LRIG1* expression have been correlated with decreased overall survival in patients with NSCLC [18-20]. We have previously shown that both transcript and protein levels of LRIG1 are lower in pre-invasive CIS lung lesions compared to donor-matched healthy epithelial tissue [18], suggesting an early role for LRIG1 during lung carcinogenesis. Here, we investigate the expression

of LRIG1 in the normal airway epithelium and examine consequences of its loss-of-function during LUSC development.

MATERIALS AND METHODS

Mouse husbandry and experimentation

Animal work was approved by the University College London Biological Services Review Committee and carried out in compliance with the UK Home Office procedural and ethical guidelines. The C57BL/6 *Lrig1::eGFP-IRES-CreERT²* murine line [21] was backcrossed twice to FVB/N. Mice were maintained in a mixed C57BL/6 and FVB/N background in individually ventilated cages, on a 12h day/night cycle with access to food and water *ad libitum*. Littermates were distributed in the appropriate experimental or control groups.

Human tissue samples

Ethical approval was obtained through the National Research Ethics Committee (REC reference 06/Q0505/12). Bronchial samples were taken during autofluorescence bronchoscopy from areas of normal bronchial epithelium. Bronchial brushes were used directly for flow cytometry and tissue biopsies frozen in OCT (Tissue-Tek 4583).

Flow cytometry

Flow cytometry was performed on a Fortessa (BD Biosciences) and cell sorting on a FACSaria (BD Biosciences). For cell cycle analysis, live cells were incubated with 1 µg/mL Hoechst 33342 for 30 minutes at 37 °C prior to antibody staining. Reagents used are indicated in Supplementary Table 1. Data was analysed using FlowJo 10.0.6 (Tree Star).

NTCU-induced LUSC model

The dorsal fur of 6-week-old female mice was shaved and 75 μ L of 0.013 M NTCU (Santa Cruz sc-212265) diluted in acetone applied twice weekly for 12 weeks. Controls received only acetone. Mice were monitored for a further 11 weeks and weighed twice weekly. On sacrifice, lungs were insufflated with 4% PFA/PBS and fixed overnight at 4°C before paraffin embedding.

Histology and immunofluorescence

Haematoxylin and eosin (H&E) staining was performed on an automated staining system (Tissue-Tek). Immunofluorescence and immunohistochemical staining were performed using standard protocols. Antigen retrieval methods, antibodies, reagents and equipment are detailed in Supplementary Methods.

Bioinformatic analyses

Analyses of the Human Lung Cell Atlas single-cell RNA sequencing (scRNAseq) dataset [22] were conducted as detailed in Supplementary Methods. We assessed *LRIG1* expression in two datasets of human pre-invasive squamous cell lung cancer lesions obtained at bronchoscopy downloaded from the Gene Expression Omnibus (GEO). The first dataset, GSE33479, contained 122 samples of pre-invasive lesions, from normal epithelium to invasive cancer, profiled using Agilent microarrays [10]. The second, GSE94611 and GSE108082, contained laser-captured epithelial samples from 51 CIS lesions (progressive and regressive) [11]. Data was analysed in the R statistical environment (v 3.5.0; www.r-project.org) using Bioconductor version 3.7.

Statistical analyses

Statistical analysis was performed on Prism 7 (GraphPad). Tests and sample sizes are indicated in figure legends; $p < 0.05$ was considered to be statistically significant.

RESULTS

LRIG1 is heterogeneously expressed in the airway epithelium

Using immunofluorescence we have previously shown LRIG1 is expressed in the murine upper airways [18]. To characterise its expression within the different cell subpopulations of the airway epithelium we used an *Lrig1* knock-in reporter mouse. In this model, a cassette encoding *eGFP-IRES-CreER^{T2}* is inserted downstream of the *Lrig1* start codon (Fig. 1a) [23]. eGFP expression occurs from the endogenous *Lrig1* promoter and results in a loss-of-function allele. As previously shown for the skin and intestine [23], antibody staining confirmed expression of eGFP recapitulates endogenous LRIG1 in the upper airways (Fig. 1b).

In both murine skin and intestinal epithelia, LRIG1 localises to defined stem cell compartments where it regulates stem cell activity [24, 25]. In contrast, *Lrig1::eGFP* expression was evident throughout the upper airway epithelium. eGFP was detected in basal (KRT5⁺), ciliated (acetylated-tubulin, ACT⁺) and, to a lesser extent, in club (SCGB1A1⁺) epithelial cells (Fig. 1b). There was no obvious enrichment of eGFP within the KRT5⁺ cell subpopulation of the submucosal glands, where a reservoir of stem cells that contribute to the regeneration of the surface epithelium after severe injury reside [26, 27] (Fig. 1b). Whole-mount immunostaining in the adult murine lung demonstrated *Lrig1::eGFP* expression extended throughout the bronchial tree, including the bronchi and bronchioles (Fig. 1c).

To determine the contribution of basal, ciliated and secretory cells to the cellular population expressing *Lrig1::eGFP* in upper airway epithelium we used flow cytometry. Tracheal epithelial cells were isolated from mice carrying one copy of the *Lrig1::eGFP* reporter allele. The immune and endothelial populations were eliminated through negative selection for CD45 and CD31, respectively. *Lrig1*⁺ epithelial cells were identified by dual expression of EPCAM and eGFP. *Griffonia simplicifolia* isolectin B4 (GSI-B4), which selectively binds to a cell surface carbohydrate found on airway basal cells [28, 29], was used to identify the basal cell population. CD24 and SSEA1 expression were used to separate ciliated and secretory cells, respectively [30] (Fig. 1d). Basal cells constituted 32.2±3.4(SEM)% of the *Lrig1::eGFP*⁺ population, whereas ciliated and secretory cells made up the 63.9±2.7% and 1.3±0.3%, respectively (Fig. 1e). The distribution of cell types did not change significantly with selection of the brightest eGFP⁺ cells (Supplementary Fig. 1), indicating *Lrig1* expression is not enriched within the basal cell compartment. Only 50.8±4.1% of the total airway basal cell population was *Lrig1::eGFP*⁺.

Murine and human basal airway epithelial cells expressing *Lrig1* have increased *in vitro* self-renewal capacity

As only a subpopulation of airway basal epithelial cells expressed *Lrig1*, we investigated whether the properties of the *Lrig1*-expressing basal cells differ from the *Lrig1*-negative subpopulation. EPCAM⁺GSI-B4⁺ airway basal epithelial cells were isolated from murine tracheas heterozygous for the *Lrig1::eGFP* allele. Cell-cycle analysis revealed the *Lrig1::eGFP*⁺ basal cell subpopulation contained a higher proportion of cells in G2/M compared to the *Lrig1::eGFP*⁻ fraction (*t*-test *p*=0.0019) (Fig. 2a & b). This agrees with previous skin and stomach findings where *Lrig1* expression identifies more proliferative stem/progenitor cell populations [21, 23, 24].

To determine whether *Lrig1*-expressing basal cells display increased self-renewal potential, we assessed their clonogenic potential in 2D culture. Freshly isolated single *Lrig1::eGFP*⁺ and *Lrig1::eGFP*⁻ basal cells from mice heterozygous for the reporter allele were sorted into 96-well plates and assessed for colony-forming ability at day 10. Basal cells expressing *Lrig1::eGFP* formed significantly more clones than those not expressing *Lrig1* (*t*-test *p*=0.013) (Fig. 2c). When seeded into Matrigel, basal airway epithelial cells give rise to 3D organoids called 'tracheospheres' [31]. Under these conditions, *Lrig1::eGFP*⁺ basal cells generated significantly more tracheospheres than *Lrig1::eGFP*⁻ cells (*t*-test *p*=0.002) (Fig. 2d & e), indicating *Lrig1*-expressing murine basal epithelial cells have higher *in vitro* propagation potential.

Next, we investigated whether LRIG1 expression identifies a more proliferative basal cell population within human airway epithelium. Examination of publicly available single-cell transcriptomic data of the human airway epithelium (www.lungcellatlas.org) [32] showed that similarly to the mouse, *LRIG1* is heterogeneously expressed by basal, ciliated and club cells (Supplementary Fig. 2). Using the scRNAseq dataset from the Human Lung Cell Atlas [22], we assessed *LRIG1* expression within the different clusters of basal cells present in the human bronchial epithelium. This revealed that *LRIG1* expression enriches for 'proliferating basal cells'. The 'basal cell' cluster, which is quiescent, was enriched in the *LRIG1*-negative fraction. Cells with a 'proximal basal' signature were present in both fractions, but appeared more abundant in the *LRIG1*⁺ one (Fig. 3a & b and Supplementary Fig. 3). Within the proliferating basal cell cluster, *LRIG1* levels

correlated with those of *MKI67*, which codes for the proliferation marker Ki67 (Pearson correlation $R=0.32$, $p=0.05$) (Fig. 3c).

Expression of LRIG1 within the KRT5⁺ basal cell compartment of the normal human bronchial epithelium was confirmed by double immunofluorescence (Fig. 3d). Normal human basal cells were isolated by flow cytometry from endobronchial brushings obtained during autofluorescence bronchoscopy. Following elimination of CD45⁺, CD31⁺ and dead cells, co-expression of the cell-surface proteins integrin alpha-6 (ITGA6) and nerve growth factor receptor (NGFR), which are enriched in airway basal cells [31] (Supplementary Fig. 4), was used to identify this cell population. Basal cells were then separated based on LRIG1 immunoreactivity (Fig. 3e). Live-cell cell-cycle analysis demonstrated an increased proportion of cells in G2/M in human basal cells expressing LRIG1 compared to the LRIG1-negative fraction (paired *t*-test $p=0.015$) (Fig. 3f). When colony-forming ability was assessed, LRIG1⁺ cells gave rise to colonies with a higher efficiency than their LRIG1⁻ counterparts (paired *t*-test $p=0.0067$) (Fig. 3g). Together, our results show that expression of LRIG1 within the basal cell compartment identifies a more proliferative cellular subpopulation with increased *in vitro* propagating potential in both murine and human airway epithelium.

LRIG1 functions as a negative regulator of EGFR signalling and thus LRIG1⁺ cells showing a greater proliferation seems paradoxical. We therefore hypothesised that LRIG1 expression is a checkpoint for proliferation employed by progenitor basal cells but not needed in a low proliferating population (LRIG1 negative). To test this, we knocked down *LRIG1* in human basal cells and indeed noted enhanced cell population expansion (Supplementary Fig. 5). Hence, LRIG1 marks a progenitor population of basal cells and functions as a checkpoint to proliferation.

Progression of pre-invasive lung cancer lesions to invasive LUSC is associated with decreased *LRIG1* expression

To better understand the role of *LRIG1* in LUSC formation, we examined expression of *LRIG1* at different stages of human LUSC development. We analysed a published dataset including patient biopsies from normal bronchial tissue, 6 morphologically distinct grades of pre-invasive disease, ranging from hyperplasia to CIS, and LUSC [10]. This revealed decreased *LRIG1* expression in pre-invasive samples that varied from metaplasia to severe dysplasia, relative to normal tissue ($p < 0.05$) (Fig. 4a). Further decline in *LRIG1* levels was observed in LUSC samples when compared to normal and hyperplastic tissue ($p = 2 \times 10^{-5}$ and $p = 0.0026$, respectively) (Fig. 4a). Additionally, assessment of *LRIG1* expression in a longitudinally characterised cohort of CIS lesions that either progressed to invasive LUSC or regressed [11] showed significantly lower *LRIG1* levels in the progressive group ($p = 0.0086$) (Fig. 4b). Together, these data indicate that a decrease of *LRIG1* expression is associated with progressive severity of pre-invasive disease through to invasive lung cancer.

Establishment of a lung squamous cell carcinoma murine model

To investigate the consequences of decreased *LRIG1* levels during LUSC development, we used a chemically induced murine model of LUSC [33]. Topical application of N-nitroso-tris-chloroethylurea (NTCU) to young-adult mice twice weekly for 12 weeks resulted in LUSC formation over the next 11 weeks (Fig. 5a). Histological analysis revealed that NTCU-induced lesions recapitulated the various stages of the human disease, from pre-invasive lesions to invasive LUSC (Fig. 5b). Pre-invasive lesions and tumours expressed the LUSC markers KRT5 and P63 and lacked expression of the lung adenocarcinoma (LUAD) marker surfactant protein C

(SPC). Rare KRT5⁺ cells expressing low levels of SCGB1A1 were detected within NTCU-induced lesions (Fig. 5c & d).

***Lrig1* loss-of-function leads to increased tumour size in a murine LUSC model**

The *Lrig1::eGFP-IRES-CreER^{T2}* knock-in allele leads to *Lrig1* loss-of-function (Fig. 6a). To establish whether decreased *Lrig1* gene dosage impacts LUSC formation, we compared effects of NTCU in *Lrig1*-null, -heterozygous and wild-type mice. Animals were monitored for weight change and there was a marked separation between the treatment and control arms from week 15 (two-way ANOVA $p < 0.05$) (Fig. 6b).

KRT5⁺ basal cells are restricted to the upper airway murine epithelium [34]. Thus, expression of KRT5 beyond the trachea and the divisions of the right and left mainstem bronchi is abnormal. Therefore, we used KRT5 immunostaining to assess the presence of pre-invasive lesions in the bronchial tree following NTCU treatment. The proportion of total bronchial tree affected by pre-invasive disease in each mouse was calculated (Fig. 6c) and compared between *Lrig1*-null, -heterozygous and wild-type mice. *Lrig1* genotype had an effect on the extent of pre-invasive disease (Kruskal-Wallis test $p = 0.033$), with the *Lrig1*-null (*Lrig1*^{-/-}) group displaying lower overall bronchial epithelial surface with abnormal KRT5 expression, when compared to *Lrig1* heterozygous (*Lrig1*^{+/-}) mice (Dunn's multiple comparisons test $p = 0.049$) (Fig. 6d). Areas of pre-invasive disease were divided according to severity into flat atypia, low-grade dysplasia and high-grade dysplasia (Table 1 & Fig. 6e & f). There were comparable proportions of both low-grade and high-grade lesions across groups (Fig. 6e). However, the presence of flat atypia, the earliest feature of pre-invasive disease, was significantly lower in the *Lrig1*-null animals when compared to

both wild-type and *Lrig1*^{+/-} mice (2-way ANOVA followed by Tukey's multiple comparisons tests; $p < 0.001$) (Fig. 6e).

We next assessed invasive tumours in the three groups. There was a trend towards increased incidence of LUSC as *Lrig1* gene dosage decreased (Chi-square test for trend $p = 0.03$) (Table 1). When we compared the frequency and size of tumours between animals with different *Lrig1* genotypes, *Lrig1* gene dosage had no significant effect on the number of tumours per individual (Fig. 6g). However, the absence of LRIG1 led to significantly larger tumours than those in mice with active LRIG1 expression (Kruskal-Wallis test $p = 0.0075$) (Fig. 6h). Larger tumours, alongside the lower frequency of flat atypia in the *Lrig1*-null lungs, suggests loss of *Lrig1* facilitates and/or accelerates pre-invasive disease progression into invasive LUSC.

To determine whether LRIG1 regulates LUSC progression by modulating cell fate or promoting proliferation, we investigated expression of P63 and Ki67 within the different spectrum of lesions. KRT5⁺ lesions were classified according to their severity and the fraction of cells expressing each marker (regardless of expression levels) were scored. The overall proportion of P63⁺ cells in NTCU-induced lung lesions was not significantly affected by *Lrig1* genotype or lesion grade (two-way ANOVA $p > 0.05$) (Fig. 7a). However, when comparisons were done only among lesions of the same grade, we found that flat atypia lesions contained a significantly higher proportion of P63⁺ cells in *Lrig1*-null mice than in their wild-type counterparts (Kruskal-Wallis test followed by Dunn's multiple comparison test $p = 0.04$). Assessment of the fraction of Ki67⁺ cells revealed differences between distinct lesion grades (two-way ANOVA, lesion grade effect $p = 0.0007$). When we evaluated genotype effects within lesions of the same grade, we found that, in comparison to

wild-type mice, mice lacking *Lrig1* also exhibited an increased fraction of Ki67⁺ cells in flat atypia lesions (Kruskal-Wallis test followed by Dunn's multiple comparison test $p=0.04$) (Fig. 7b). This suggests that LRIG1 activity restrains LUSC formation by restricting progenitor cell proliferation in early pre-invasive disease.

DISCUSSION

Studies of the homeostatic upper airway epithelium in mouse and human highlight phenotypic and functional heterogeneity within the basal cell compartment. Current evidence indicates basal cells comprise a population of multipotent stem cells and committed progenitors [32, 35-37]. Here we find that *Lrig1* is heterogeneously expressed in the airway epithelium and its expression identifies a more proliferative subpopulation of basal cells with increased *in vitro* self-renewal potential. These findings are in line with previous studies in the epidermis and forestomach, where LRIG1 expression marks proliferative epithelial stem/progenitor cells, and in glandular gastric epithelial cells, where *Lrig1*-expressing cells have higher organoid-forming ability than their *Lrig1*-negative counterparts [21, 23]. This suggests a conserved role for LRIG1 in regulation of progenitor cell activity in distinct epithelia.

In contrast to the skin and intestine, where *Lrig1* is enriched in the stem cell compartment [24, 25], in the murine gastric epithelium *Lrig1* is expressed by both progenitor and differentiated cells [23, 38]. Similarly, we find that in the upper airways, expression of *Lrig1* is detected in basal, ciliated and secretory cells. In the mouse distal airways, scRNAseq analyses have shown that *Lrig1* is enriched in SCGB1A1⁺ club cells and expressed at moderate levels by SPC⁺SCGB1A1⁺ bronchioalveolar stem cells (BASCs) [39]. Analogous studies of the human airways show that *LRIG1* is heterogeneously expressed across the different epithelial cell

subpopulations [32]. This raises the possibility that LRIG1 may exert functional roles in airway epithelial stem cells, lineage-restricted progenitors and differentiated cells. In future studies it would be important to determine how LRIG1 dysregulation affects these different populations using lineage-specific loss- or gain-of-function approaches.

Dysregulation of LRIG1 is seen across different tumour types [40]. Decreased *LRIG1* expression has been associated with poor prognosis in a range of epithelial tumours, including lung cancer [19, 20, 41]. We now show downregulation of *LRIG1* occurs early during LUSC evolution, before development of high-grade lesions and invasive tumours. Primary human pre-invasive squamous lung cancer has not been grown in culture, limiting functional investigation of the molecular alterations occurring at this stage of LUSC development. Here we find that *LRIG1* knockdown enhances *in vitro* propagation of primary basal cells isolated from the human normal airway epithelium, supporting a potential regulatory role in pre-invasive disease development. Recently, air liquid interface cultures of immortalised human bronchial epithelial cells with loss of *TP53* and *SOX2* overexpression have been shown to recapitulate bronchial dysplasia features [42]. This model may be useful to assess the consequences of loss of *LRIG1* in pre-invasive squamous cancer in future studies.

In an NTCU-induced murine model of LUSC, we found a trend towards increased LUSC development as *Lrig1* gene dosage decreased. The absence of *Lrig1* led to decreased presence of flat atypia and formation of larger invasive tumours. A correlation between lower LRIG1 expression and increased tumour size has been previously identified in hepatocellular carcinoma [43]. Gain- and loss-of-function studies in cancer cell lines from lung, breast and liver indicate that LRIG1 modulates

cancer cell proliferation [43-45]. Assessment of Ki67 expression in NTCU-induced lesions showed that *Lrig1* depletion leads to abnormally high proliferative rates in early flat atypia lesions, but not in dysplasia or invasive tumours. These observations suggest the larger tumours in the *Lrig1*-null lungs result from accelerated disease progression, rather than from increased cell proliferation in established tumours.

We have shown that LRIG1 exerts a tumour suppressive role in LUSC development. Therefore, *LRIG1* loss may be used as a biomarker of poor outcome of pre-invasive lesions and lead to a lower threshold for intervention. With the loss of the break of LRIG1 in EGFR signalling contributing to the development of pre-invasive disease, our work highlights a potential role for EGFR antagonists in LUSC prevention. Other data suggests a key role in the suppression of LUAD. As a negative regulator of EGFR signalling, high LRIG1 expression is associated with a dramatic 2.8 year improved survival in LUAD patients [20]. Decreased *LRIG1* transcript levels have been reported in LUAD cell lines, especially those with mutant EGFR [44]. Transfection of EGFR mutant LUAD cells with *LRIG1* led to decreased proliferation, invasion and migratory potential [44].

To date, functional analyses of the role of LRIG1 in NSCLC had relied on *in vitro* studies and xenograft models using LUAD cell lines [18, 44]. Here, we have used a chemically induced model of LUSC that develops endogenous cancer lesions recapitulating the histopathological features of the human disease, including step-wise progression through pre-invasive stages. RNA sequencing analyses of NTCU-induced tumours indicate their transcriptional landscape mimics human LUSC [46], supporting the relevance of this model for understanding LUSC progression. We show that using NTCU-induced carcinogenesis in the context of a transgenic murine

model enables assessment of gene function during different stages of LUSC development and provides a system for validating candidate tumour suppressors, oncogenes and therapeutic targets for the prevention and treatment of LUSC.

ACKNOWLEDGEMENTS

We want to thank Angela Barrett, Marie-Belle El Mdawar and Robert Hynds (University College London, London, UK) for assisting with quantitative analyses, support with human cell culture and technical advice, respectively.

SUPPORT STATEMENT

S.M.J. was a Wellcome Trust Senior Fellow in Clinical Science (WT107963AIA) and is supported by a CRUK programme award, the Roy Castle Lung Cancer Foundation, the Rosetrees Trust, UCLH Charitable Foundation, the Longfonds BREATH consortium and the MRC UKRMP2 cell therapy platform. L.S. was supported by a CRUK Clinical Research fellowship and a Wellcome Trust clinical PhD training fellowship. S.G.-L. was supported by a Royal Society Newton International Fellowship (NF161172). A.P. was funded by a Wellcome Trust clinical PhD training fellowship. This work was partially undertaken at UCLH/UCL who received a proportion of funding from the Department of Health's NIHR Biomedical Research Centre's funding scheme. The Novo Nordisk Foundation Center for Stem Cell Biology is supported by Novo Nordisk Foundation grant (NNF17CC0027852).

CONFLICT OF INTEREST

The authors declare no conflicts of interest relating to this study.

AUTHOR CONTRIBUTIONS

L.S. and S.G.-L. performed experiments, analysed data and co-wrote the manuscript with input from S.M.J. A.P. and A.S.N.A. performed bioinformatic studies. D.D. executed cell sorting experiments. S.E.C. and K.H.C.G. contributed to studies with human bronchial epithelial cells. N.A.W. performed pathology assessment. K.B.J. provided the *Lrig1::eGFP-IRES-CreERT²* murine line and expert advice throughout the study. L.S. and S.M.J. designed the study. S.M.J. supervised the study. All authors approved the final version of the manuscript.

REFERENCES

1. Bray F, Ferlay J, Soerjomataram I, Siegel RL, Torre LA, Jemal A. Global cancer statistics 2018: GLOBOCAN estimates of incidence and mortality worldwide for 36 cancers in 185 countries. *CA: a cancer journal for clinicians* 2018; 68(6): 394-424.
2. Cheng TY, Cramb SM, Baade PD, Youlden DR, Nwogu C, Reid ME. The International Epidemiology of Lung Cancer: Latest Trends, Disparities, and Tumor Characteristics. *Journal of thoracic oncology : official publication of the International Association for the Study of Lung Cancer* 2016; 11(10): 1653-1671.
3. Youlden DR, Cramb SM, Baade PD. The International Epidemiology of Lung Cancer: geographical distribution and secular trends. *Journal of thoracic oncology : official publication of the International Association for the Study of Lung Cancer* 2008; 3(8): 819-831.
4. Herbst RS, Morgensztern D, Boshoff C. The biology and management of non-small cell lung cancer. *Nature* 2018; 553(7689): 446-454.
5. Auerbach O, Stout AP, Hammond EC, Garfinkel L. Changes in bronchial epithelium in relation to cigarette smoking and in relation to lung cancer. *The New England journal of medicine* 1961; 265: 253-267.
6. Nicholson AG, Perry LJ, Cury PM, Jackson P, McCormick CM, Corrin B, Wells AU. Reproducibility of the WHO/IASLC grading system for pre-invasive squamous lesions of the bronchus: a study of inter-observer and intra-observer variation. *Histopathology* 2001; 38(3): 202-208.
7. de Groot P, Munden RF. Lung cancer epidemiology, risk factors, and prevention. *Radiologic clinics of North America* 2012; 50(5): 863-876.
8. Yoshida K, Gowers KHC, Lee-Six H, Chandrasekharan DP, Coorens T, Maughan EF, Beal K, Menzies A, Millar FR, Anderson E, Clarke SE, Pennycuick A, Thakrar RM, Butler CR, Kakiuchi N, Hirano T, Hynds RE, Stratton MR, Martincorena I, Janes SM, Campbell PJ. Tobacco smoking and somatic mutations in human bronchial epithelium. *Nature* 2020; 578(7794): 266-272.
9. Beane JE, Mazzilli SA, Campbell JD, Duclos G, Krysan K, Moy C, Perdomo C, Schaffer M, Liu G, Zhang S, Liu H, Vick J, Dhillon SS, Platero SJ, Dubinett SM, Stevenson C, Reid ME, Lenburg ME, Spira AE. Molecular subtyping reveals immune alterations associated with progression of bronchial premalignant lesions. *Nat Commun* 2019; 10(1): 1856.
10. Mascaux C, Angelova M, Vasaturo A, Beane J, Hijazi K, Anthoine G, Buttard B, Rothe F, Willard-Gallo K, Haller A, Ninane V, Burny A, Sculier JP, Spira A, Galon J. Immune evasion before tumour invasion in early lung squamous carcinogenesis. *Nature* 2019.
11. Teixeira VH, Pipinikas CP, Pennycuick A, Lee-Six H, Chandrasekharan D, Beane J, Morris TJ, Karpathakis A, Feber A, Breeze CE, Ntoliou P, Hynds RE, Falzon M, Capitanio A, Carroll B, Durrenberger PF, Hardavella G, Brown JM, Lynch AG, Farmery H, Paul DS, Chambers RC, McGranahan N, Navani N, Thakrar RM, Swanton C, Beck S, George PJ, Spira A, Campbell PJ, Thirlwell C, Janes SM. Deciphering the genomic, epigenomic, and transcriptomic landscapes of pre-invasive lung cancer lesions. *Nat Med* 2019; 25(3): 517-525.
12. van Boerdonk RA, Sutedja TG, Snijders PJ, Reinen E, Wilting SM, van de Wiel MA, Thunnissen FE, Duin S, Kooi C, Ylstra B, Meijer CJ, Meijer GA, Grunberg K, Daniels JM, Postmus PE, Smit EF, Heideman DA. DNA copy number alterations in endobronchial squamous metaplastic lesions predict lung cancer. *Am J Respir Crit Care Med* 2011; 184(8): 948-956.

13. Pennycuik A, Teixeira VH, AbdulJabbar K, Raza SEA, Lund T, Akarca AU, Rosenthal R, Kalinke L, Chandrasekharan DP, Pipinikas CP, Lee-Six H, Hynds RE, Gowers KHC, Henry JY, Millar FR, Hagos YB, Denais C, Falzon M, Moore DA, Antoniou S, Durrenberger PF, Furness AJ, Carroll B, Marceaux C, Asselin-Labat ML, Larson W, Betts C, Coussens LM, Thakrar RM, George J, Swanton C, Thirlwell C, Campbell PJ, Marafioti T, Yuan Y, Quezada SA, McGranahan N, Janes SM. Immune Surveillance in Clinical Regression of Preinvasive Squamous Cell Lung Cancer. *Cancer Discov* 2020; 10(10): 1489-1499.
14. Laederich MB, Funes-Duran M, Yen L, Ingalla E, Wu X, Carraway KL, 3rd, Sweeney C. The leucine-rich repeat protein LRIG1 is a negative regulator of ErbB family receptor tyrosine kinases. *The Journal of biological chemistry* 2004; 279(45): 47050-47056.
15. Gur G, Rubin C, Katz M, Amit I, Citri A, Nilsson J, Amariglio N, Henriksson R, Rechavi G, Hedman H, Wides R, Yarden Y. LRIG1 restricts growth factor signaling by enhancing receptor ubiquitylation and degradation. *The EMBO journal* 2004; 23(16): 3270-3281.
16. Viegas-Pequignot E, Flury-Herard A, De Cremoux H, Chlecq C, Bignon J, Dutrillaux B. Recurrent chromosome aberrations in human lung squamous cell carcinomas. *Cancer genetics and cytogenetics* 1990; 49(1): 37-49.
17. Sundaresan V, Ganly P, Hasleton P, Rudd R, Sinha G, Bleehen NM, Rabbitts P. p53 and chromosome 3 abnormalities, characteristic of malignant lung tumours, are detectable in preinvasive lesions of the bronchus. *Oncogene* 1992; 7(10): 1989-1997.
18. Lu L, Teixeira VH, Yuan Z, Graham TA, Endesfelder D, Kolluri K, Al-Juffali N, Hamilton N, Nicholson AG, Falzon M, Kschischo M, Swanton C, Wright NA, Carroll B, Watt FM, George JP, Jensen KB, Giangreco A, Janes SM. LRIG1 regulates cadherin-dependent contact inhibition directing epithelial homeostasis and pre-invasive squamous cell carcinoma development. *J Pathol* 2013; 229(4): 608-620.
19. An Y, Zhao Z, Ou P, Wang G. Expression of LRIG1 is Associated With Good Prognosis for Human Non-small Cell Lung Cancer. *Medicine* 2015; 94(47): e2081.
20. Kvarnbrink S, Karlsson T, Edlund K, Botling J, Lindquist D, Jirstrom K, Micke P, Henriksson R, Johansson M, Hedman H. LRIG1 is a prognostic biomarker in non-small cell lung cancer. *Acta oncologica (Stockholm, Sweden)* 2015; 54(8): 1113-1119.
21. Page ME, Lombard P, Ng F, Gottgens B, Jensen KB. The epidermis comprises autonomous compartments maintained by distinct stem cell populations. *Cell Stem Cell* 2013; 13(4): 471-482.
22. Travaglini KJ, Nabhan AN, Penland L, Sinha R, Gillich A, Sit RV, Chang S, Conley SD, Mori Y, Seita J, Berry GJ, Shrager JB, Metzger RJ, Kuo CS, Neff N, Weissman IL, Quake SR, Krasnow MA. A molecular cell atlas of the human lung from single-cell RNA sequencing. *Nature* 2020; 587(7835): 619-625.
23. Schweiger PJ, Clement DL, Page ME, Schepeler T, Zou X, Sirokmany G, Watt FM, Jensen KB. Lrig1 marks a population of gastric epithelial cells capable of long-term tissue maintenance and growth in vitro. *Sci Rep* 2018; 8(1): 15255.
24. Wong VW, Stange DE, Page ME, Buczacki S, Wabik A, Itami S, van de Wetering M, Poulson R, Wright NA, Trotter MW, Watt FM, Winton DJ, Clevers H, Jensen KB. Lrig1 controls intestinal stem-cell homeostasis by negative regulation of ErbB signalling. *Nat Cell Biol* 2012; 14(4): 401-408.
25. Jensen KB, Collins CA, Nascimento E, Tan DW, Frye M, Itami S, Watt FM. Lrig1 expression defines a distinct multipotent stem cell population in mammalian epidermis. *Cell Stem Cell* 2009; 4(5): 427-439.

26. Tata A, Kobayashi Y, Chow RD, Tran J, Desai A, Massri AJ, McCord TJ, Gunn MD, Tata PR. Myoepithelial Cells of Submucosal Glands Can Function as Reserve Stem Cells to Regenerate Airways after Injury. *Cell Stem Cell* 2018: 22(5): 668-683.e666.
27. Lynch TJ, Anderson PJ, Rotti PG, Tyler SR, Crooke AK, Choi SH, Montoro DT, Silverman CL, Shahin W, Zhao R, Jensen-Cody CW, Adamcakova-Dodd A, Evans TIA, Xie W, Zhang Y, Mou H, Herring BP, Thorne PS, Rajagopal J, Yeaman C, Parekh KR, Engelhardt JF. Submucosal Gland Myoepithelial Cells Are Reserve Stem Cells That Can Regenerate Mouse Tracheal Epithelium. *Cell Stem Cell* 2018: 22(5): 653-667.e655.
28. Schoch KG, Lori A, Burns KA, Eldred T, Olsen JC, Randell SH. A subset of mouse tracheal epithelial basal cells generates large colonies in vitro. *Am J Physiol Lung Cell Mol Physiol* 2004: 286(4): L631-642.
29. Shimizu T, Nettesheim P, Mahler JF, Randell SH. Cell type-specific lectin staining of the tracheobronchial epithelium of the rat: quantitative studies with Griffonia simplicifolia I isolectin B4. *The journal of histochemistry and cytochemistry : official journal of the Histochemistry Society* 1991: 39(1): 7-14.
30. Tata PR, Mou H, Pardo-Saganta A, Zhao R, Prabhu M, Law BM, Vinarsky V, Cho JL, Breton S, Sahay A, Medoff BD, Rajagopal J. Dedifferentiation of committed epithelial cells into stem cells in vivo. *Nature* 2013: 503(7475): 218-223.
31. Rock JR, Onaitis MW, Rawlins EL, Lu Y, Clark CP, Xue Y, Randell SH, Hogan BL. Basal cells as stem cells of the mouse trachea and human airway epithelium. *Proc Natl Acad Sci U S A* 2009: 106(31): 12771-12775.
32. Vieira Braga FA, Kar G, Berg M, Carpaij OA, Polanski K, Simon LM, Brouwer S, Gomes T, Hesse L, Jiang J, Fasouli ES, Efremova M, Vento-Tormo R, Talavera-Lopez C, Jonker MR, Affleck K, Palit S, Strzelecka PM, Firth HV, Mahubani KT, Cvejic A, Meyer KB, Saeb-Parsy K, Luinge M, Brandsma CA, Timens W, Angelidis I, Strunz M, Koppelman GH, van Oosterhout AJ, Schiller HB, Theis FJ, van den Berge M, Nawijn MC, Teichmann SA. A cellular census of human lungs identifies novel cell states in health and in asthma. *Nat Med* 2019: 25(7): 1153-1163.
33. Wang Y, Zhang Z, Yan Y, Lemon WJ, LaRegina M, Morrison C, Lubet R, You M. A chemically induced model for squamous cell carcinoma of the lung in mice: histopathology and strain susceptibility. *Cancer Res* 2004: 64(5): 1647-1654.
34. Rock JR, Randell SH, Hogan BL. Airway basal stem cells: a perspective on their roles in epithelial homeostasis and remodeling. *Dis Model Mech* 2010: 3(9-10): 545-556.
35. Pardo-Saganta A, Law BM, Tata PR, Villoria J, Saez B, Mou H, Zhao R, Rajagopal J. Injury induces direct lineage segregation of functionally distinct airway basal stem/progenitor cell subpopulations. *Cell Stem Cell* 2015: 16(2): 184-197.
36. Watson JK, Rulands S, Wilkinson AC, Wuidart A, Ousset M, Van Keymeulen A, Gottgens B, Blanpain C, Simons BD, Rawlins EL. Clonal Dynamics Reveal Two Distinct Populations of Basal Cells in Slow-Turnover Airway Epithelium. *Cell Rep* 2015: 12(1): 90-101.
37. Plasschaert LW, Zilionis R, Choo-Wing R, Savova V, Knehr J, Roma G, Klein AM, Jaffe AB. A single-cell atlas of the airway epithelium reveals the CFTR-rich pulmonary ionocyte. *Nature* 2018: 560(7718): 377-381.
38. Choi E, Lantz TL, Vlacich G, Keeley TM, Samuelson LC, Coffey RJ, Goldenring JR, Powell AE. Lrig1+ gastric isthmal progenitor cells restore normal gastric lineage cells during damage recovery in adult mouse stomach. *Gut* 2018: 67(9): 1595-1605.

39. Liu Q, Liu K, Cui G, Huang X, Yao S, Guo W, Qin Z, Li Y, Yang R, Pu W, Zhang L, He L, Zhao H, Yu W, Tang M, Tian X, Cai D, Nie Y, Hu S, Ren T, Qiao Z, Huang H, Zeng YA, Jing N, Peng G, Ji H, Zhou B. Lung regeneration by multipotent stem cells residing at the bronchioalveolar-duct junction. *Nat Genet* 2019; 51(4): 728-738.
40. Lindquist D, Kvarnbrink S, Henriksson R, Hedman H. LRIG and cancer prognosis. *Acta oncologica (Stockholm, Sweden)* 2014; 53(9): 1135-1142.
41. Rouam S, Moreau T, Broet P. Identifying common prognostic factors in genomic cancer studies: a novel index for censored outcomes. *BMC bioinformatics* 2010; 11: 150.
42. Correia LL, Johnson JA, McErlean P, Bauer J, Farah H, Rassl DM, Rintoul RC, Sethi T, Lavender P, Rawlins EL, Littlewood TD, Evan GI, McCaughan FM. SOX2 Drives Bronchial Dysplasia in a Novel Organotypic Model of Early Human Squamous Lung Cancer. *Am J Respir Crit Care Med* 2017; 195(11): 1494-1508.
43. Yang B, Dai C, Tan R, Zhang B, Meng X, Ye J, Wang X, Wei L, He F, Chen Z. Lrig1 is a positive prognostic marker in hepatocellular carcinoma. *OncoTargets and therapy* 2016; 9: 7071-7079.
44. Torigoe H, Yamamoto H, Sakaguchi M, Youyi C, Namba K, Sato H, Shien K, Soh J, Suzawa K, Tomida S, Tsukuda K, Miyoshi S, Toyooka S. Tumor-suppressive effect of LRIG1, a negative regulator of ErbB, in non-small cell lung cancer harboring mutant EGFR. *Carcinogenesis* 2018; 39(5): 719-727.
45. Miller JK, Shattuck DL, Ingalla EQ, Yen L, Borowsky AD, Young LJ, Cardiff RD, Carraway KL, 3rd, Sweeney C. Suppression of the negative regulator LRIG1 contributes to ErbB2 overexpression in breast cancer. *Cancer Res* 2008; 68(20): 8286-8294.
46. Riobos L, Gad EA, Treuting PM, Timms AE, Hershberg EA, Corulli LR, Rodmaker E, Disis ML. The Effect of Mouse Strain, Sex, and Carcinogen Dose on Toxicity and the Development of Lung Dysplasia and Squamous Cell Carcinomas in Mice. *Cancer Prev Res (Phila)* 2019; 12(8): 507-516.

TABLES

Table 1. Incidence of NTCU-induced pre-invasive lesions and LUSC in *Lrig1*-deficient and control mice.

	% Incidence (animals with lesions/total number of animals)			
<i>Lrig1</i> genotype	Flat atypia (n)	Low-grade (n)	High-grade (n)	LUSC (n)
+/+	100% (11/11)	100% (11/11)	90.90% (10/11)	36.36% (4/11)
+/-	100% (9/9)	100% (9/9)	88.89% (8/9)	66.67% (6/9)
-/-	100% (7/7)	100% (7/7)	85.71% (6/7)	85.71% (6/7)

FIGURE LEGENDS

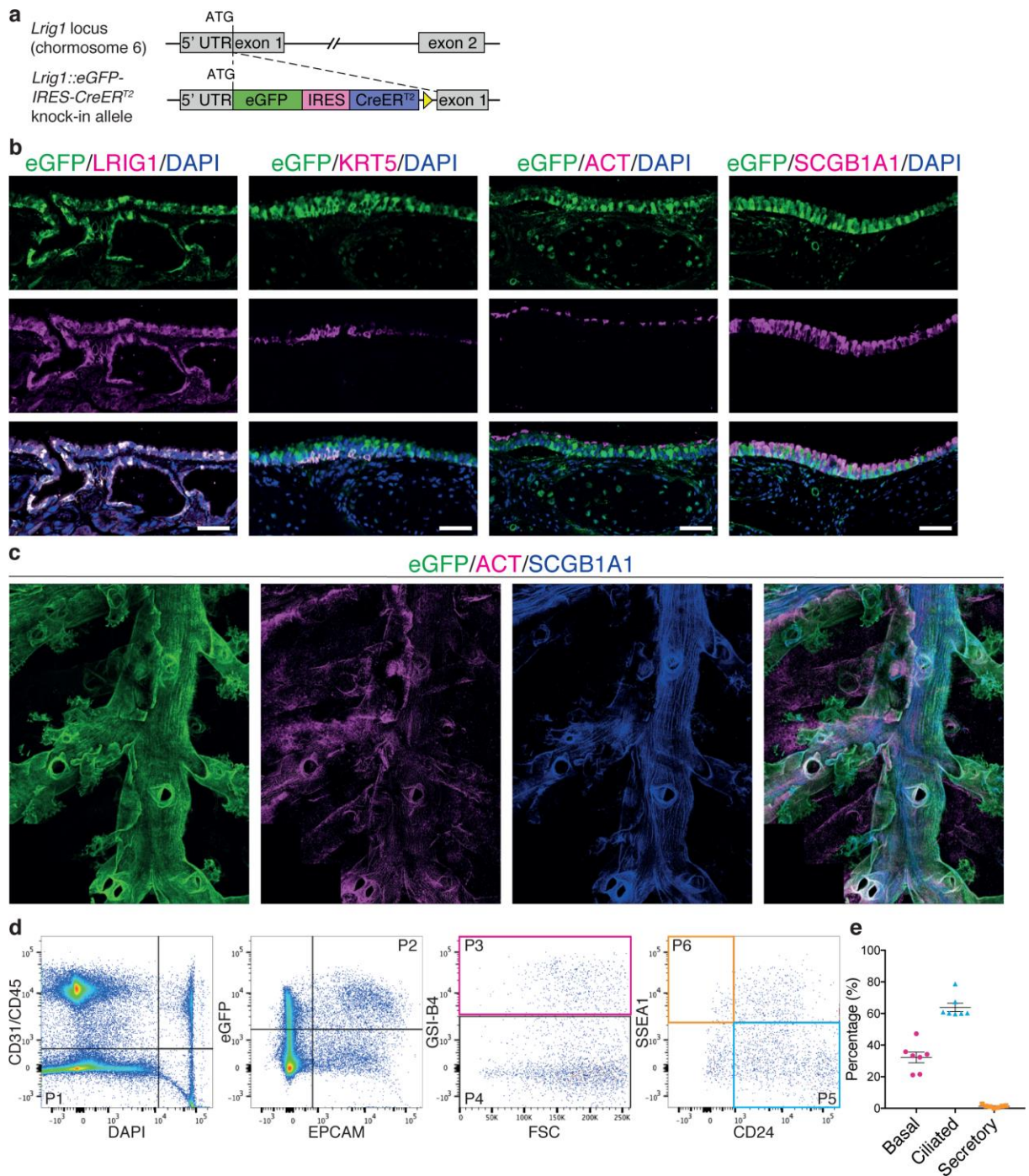


Figure 1. Expression of *Lrig1* in the murine airways. **(a)** Schematic representation of wild-type and knock-in reporter *Lrig1* alleles. An eGFP-IRES-CreER^{T2} cassette was targeted to the start codon of *Lrig1*, shifting the endogenous gene out of frame. **(b)** Immunofluorescence images of tracheal sections from mice heterozygous for the knock-in reporter *Lrig1* allele demonstrate that expression of eGFP (green)

recapitulates endogenous LRIG1 protein (magenta). Expression of eGFP is detected in different cell compartments of the airway epithelium, including KRT5⁺ basal cells, ACT⁺ ciliated cells and SCGB1A1⁺ secretory cells. Scale bars represent 50 μ m. **(c)** Whole-mount preparation of an adult mouse lung showing expression of eGFP in the lung airways. Antibody staining for SCGB1A1 and ACT was used for identification of club and ciliated cells, respectively. **(d)** Immunophenotypic characterisation of tracheal epithelial cells expressing *Lrig1::eGFP* by flow cytometry. Live tracheal epithelial cells (P1) were identified by negative selection of cells expressing CD31, CD45 (endothelial cells and lymphocytes) and DAPI, followed by positive selection of EPCAM⁺eGFP⁺ cells (P2). GSI-B4 labelling was used to distinguish basal cells (P3) within the EPCAM⁺eGFP⁺ population. Ciliated and secretory cells were selected within the GSI-B4-negative fraction by expression of CD24 (P5) and SSEA1 (P6), respectively. **(e)** Distribution of cell types in the eGFP⁺ tracheal epithelium (mean \pm SEM, $n=7$).

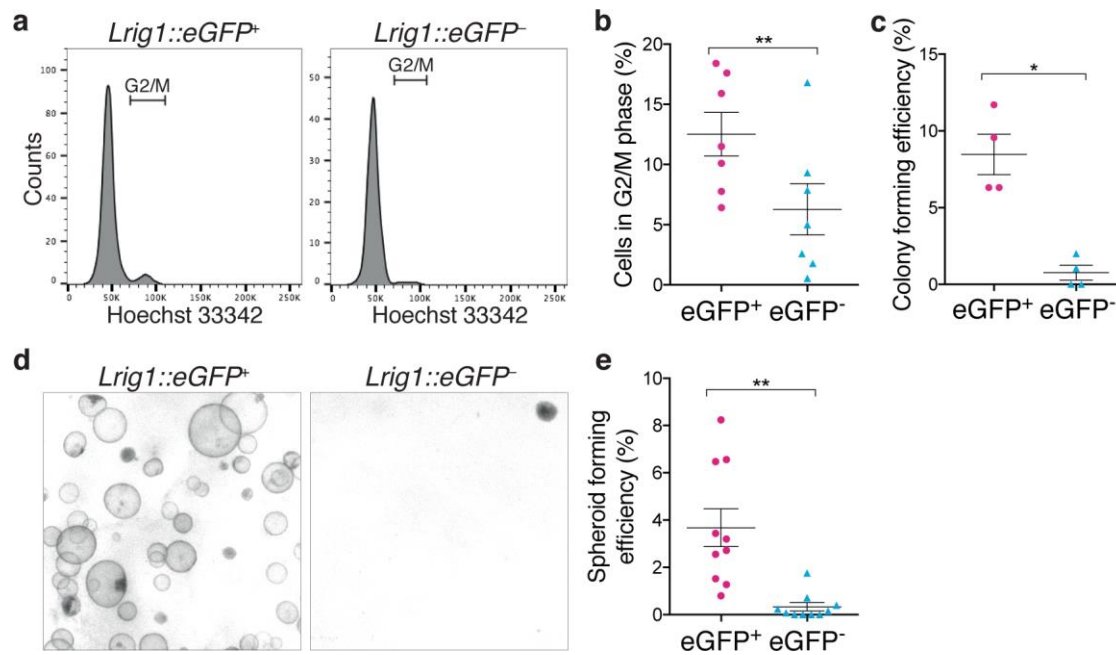


Figure 2. Mouse basal airway epithelial cells expressing LRIG1 have increased *in vitro* self-renewal potential. **(a)** EPCAM⁺GSI-B4⁺ basal murine airway epithelial cells from *Lrig1::eGFP* heterozygous mice were purified by flow cytometry from freshly dissociated tissue following depletion of the CD31⁺ and CD45⁺ populations. Hoechst 33342 staining was used to compare DNA content in the eGFP-positive and negative fractions. **(b)** The proportion of cells in G2/M phase is higher in eGFP⁺ basal cells compared to eGFP⁻ basal cells (mean±SEM, ***t*-test $p=0.0019$, $n=7$ biological replicates). **(c)** Single eGFP⁺ or eGFP⁻ basal cells were sorted by flow-cytometry into individual wells of 96-well plates containing mitotically inactivated feeder cells. The number of cells giving rise to colonies containing more than 10 cells was assessed 10 days after plating (*paired *t*-test $p=0.013$, $n=4$ mice). **(d & e)** The ability of eGFP⁺ and eGFP⁻ basal cells to form spheroids was assessed following 14 days of culture in Matrigel (mean±SEM, **paired *t*-test $p<0.002$, $n=10$ mice).

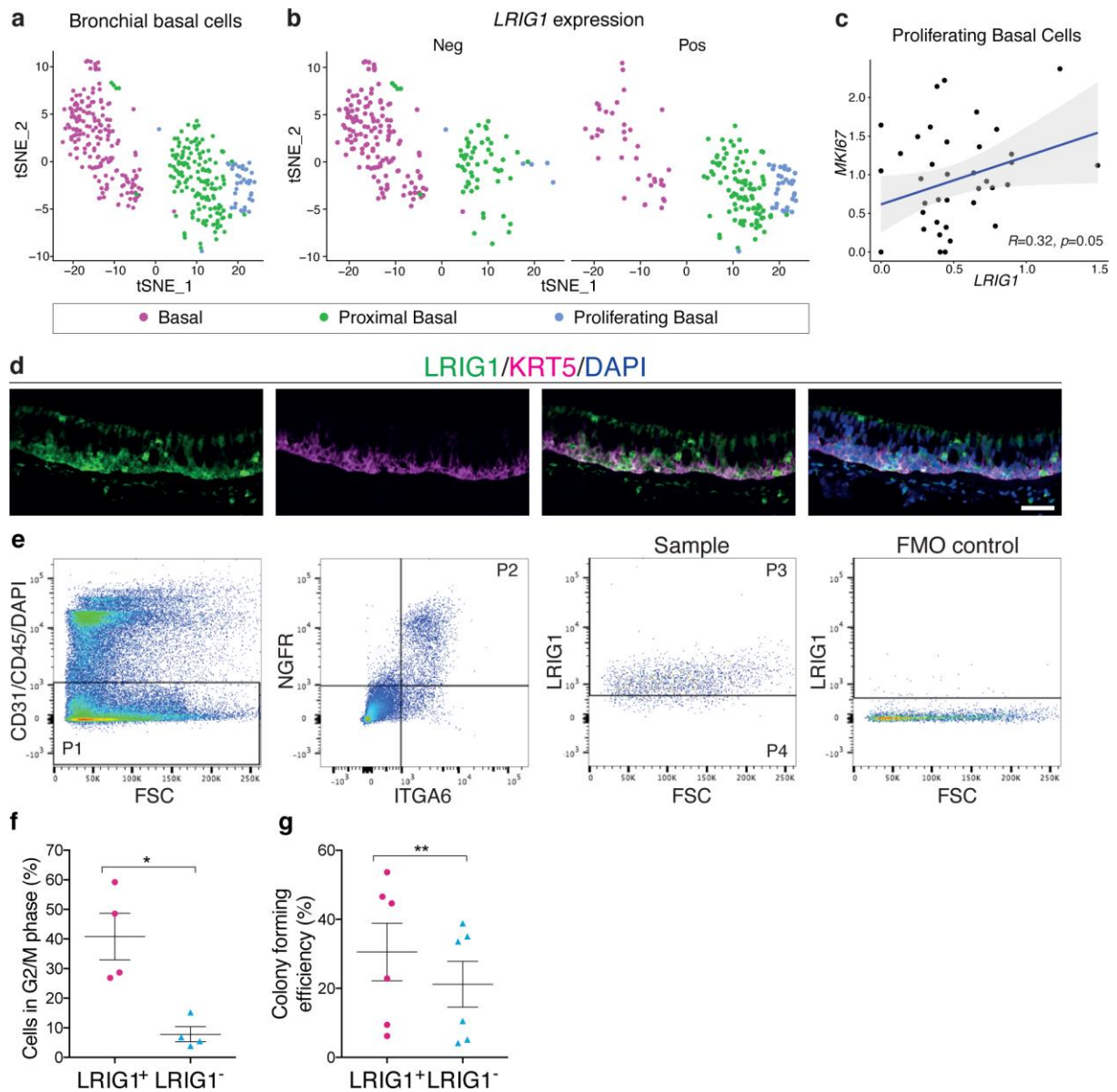


Figure 3. Expression of *LRIG1* in human basal airway epithelial cells is associated with increased proliferation. The scRNAseq dataset from the Human Lung Cell Atlas was used to examine differences between bronchial basal cells with or without *LRIG1* expression. **(a)** tSNE dimensional reductions displaying the major basal cell clusters present in bronchial regions. **(b)** Count of cells with (Pos) or without (Neg) *LRIG1* expression in each basal cell subpopulation. **(c)** Scatter plot displaying the correlation between *LRIG1* and *MKI67* expression in proliferating basal cells from the Human Lung Cell Atlas. **(d)** Immunofluorescence staining for *LRIG1* and the basal cell

marker KRT5 in the human airway epithelium. Scale bar represents 50 μm . **(e)** ITGA6⁺NGFR⁺ human basal cells (P2) were isolated from endobronchial brushings by flow cytometry and separated into LRIG1⁺ (P3) and LRIG1⁻ (P4) subpopulations. Fluorescence minus one (FMO) control is shown. **(f)** Cell-cycle analysis on live cells using Hoechst 33342 indicates that the LRIG1⁺ human basal cell fraction contains an increased proportion of cells in G2/M (mean \pm SEM, *paired *t*-test $p=0.0153$, $n=4$ patients). **(g)** The proportion of individual LRIG1⁺ and LRIG1⁻ human basal cells giving rise to colonies after 10 days of culture on mitotically inactivated feeder cells is shown (mean \pm SEM, **paired *t*-test $p=0.0067$, $n=6$ patients).

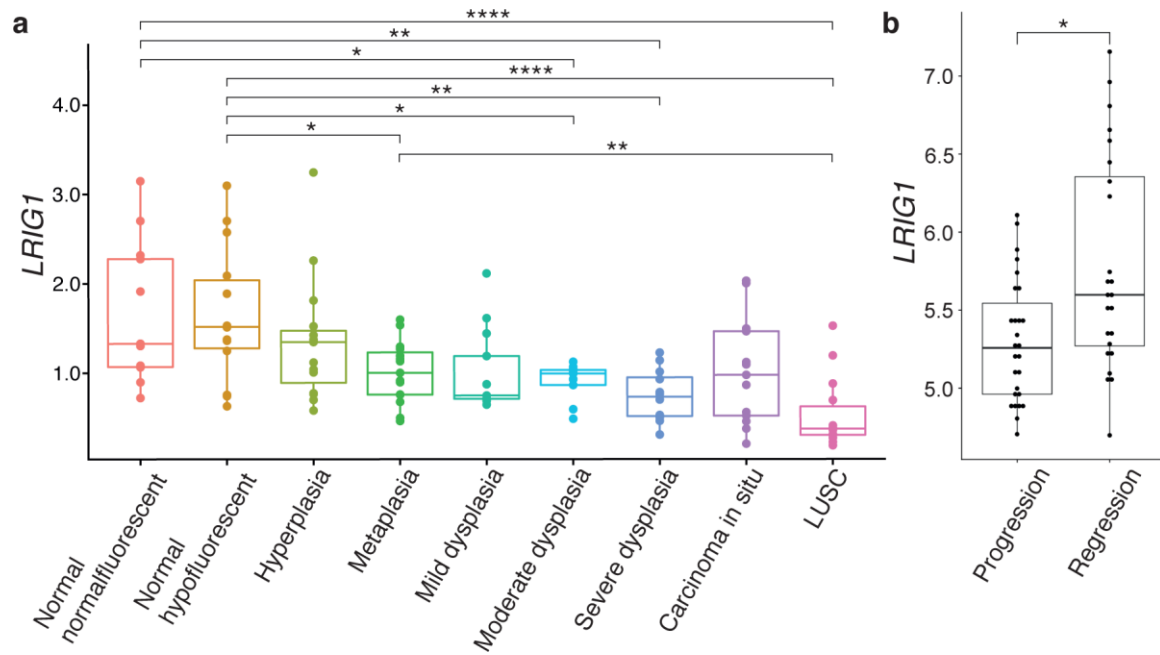


Figure 4. Expression of *LRIG1* during human LUSC progression. **(a)** Comparison of *LRIG1* gene expression in 122 pre-invasive squamous cell lung cancer lesions across stages of progression to cancer, as defined by standard histological criteria. ANOVA $p=3.7 \times 10^{-7}$, Tukey's multiple comparisons test was used for between-group analysis. * $p < 0.05$, ** $p < 0.005$, **** $p < 0.0005$. **(b)** Analysis of *LRIG1* expression data from laser-captured CIS lesions that either progressed to cancer ($n=27$) or spontaneously regressed ($n=24$), showing decreased expression of *LRIG1* in those that progressed to cancer. * $p=0.0086$ (Wilcoxon rank sum test).

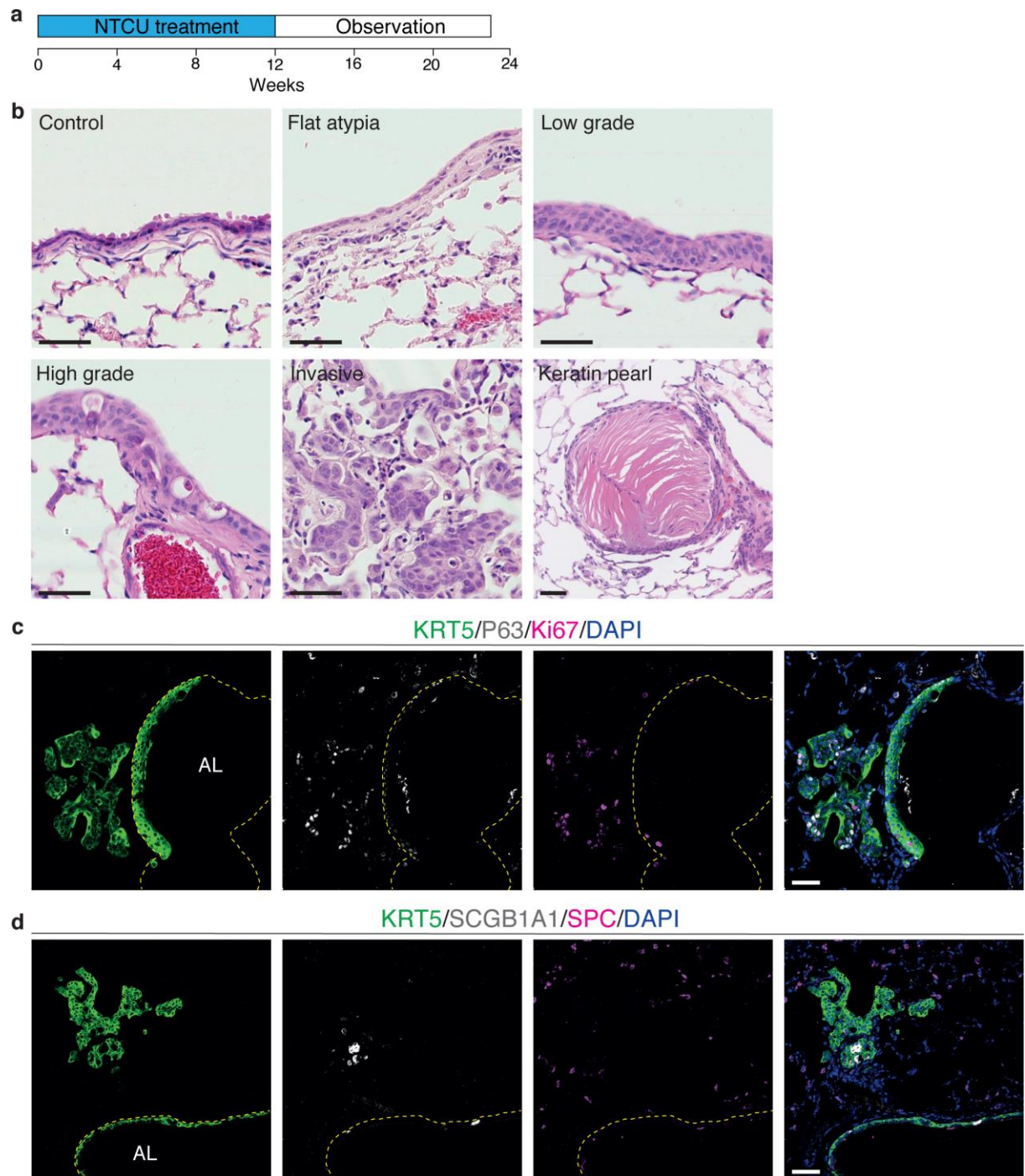


Figure 5. NTCU-induced murine lung squamous cell carcinoma. **(a)** NTCU administration protocol for the induction of murine lung squamous cell carcinoma. **(b)** Representative images of NTCU-induced lung lesions stained with H&E. Flat atypia with enlarged, flattened nuclei and increased nuclear-cytoplasmic ratio. Low-grade dysplasia with presence of multiple, ordered layers of epithelial cells and clear

organisation from the basement membrane to the luminal surface. Note flattened nuclei adjacent to the lumen. High-grade dysplasia showing disordered layers of epithelial cells and multiple enlarged nuclei. Invasive squamous cell carcinoma lesion, beginning to fill the alveolar spaces. Keratin pearl, a characteristic feature of squamous cell carcinoma. Scale bars represent 50 μm . **(c)** Immunofluorescence staining showing expression of the lung squamous cell carcinoma markers P63 and KRT5, and the proliferation marker Ki67, in NTCU-induced lesions. **(d)** Antibody staining demonstrates lack of immunoreactivity for the LUAD marker SPC within NTCU-induced lesions. Basement membrane (dashed lines) and airway lumen (AL) are indicated. Scale bars represent 50 μm .

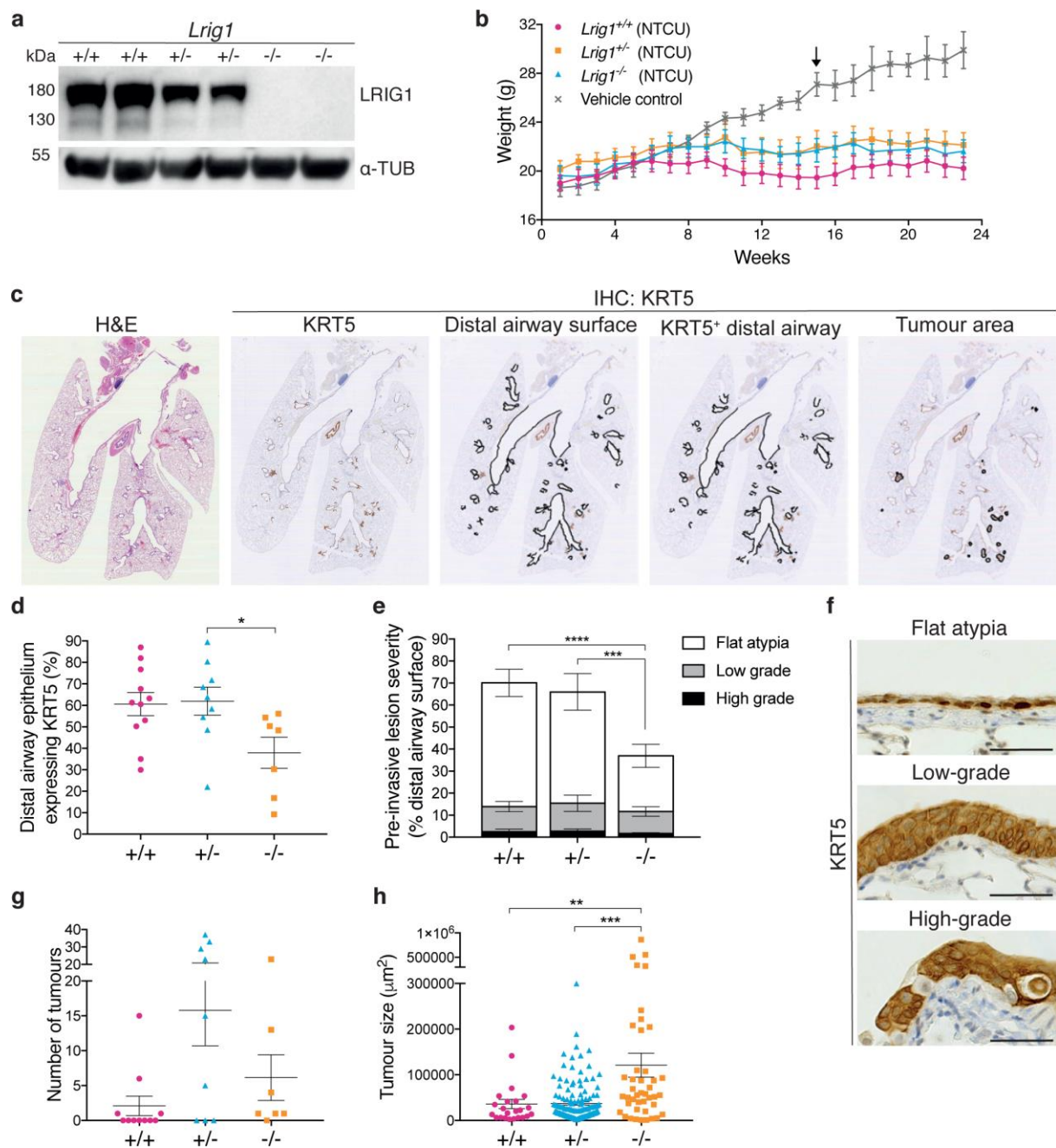


Figure 6. Effects of *Lrig1* loss-of-function on NTCU-induced lung carcinogenesis. **(a)** Immunoblot for LRIG1 on cerebellar tissue lysates from wild-type, *Lrig1*-heterozygous and *Lrig1*-null mice. Note that protein levels change in a gene-dosage dependent manner. α -tubulin is shown as a loading control. **(b)** Weights of NTCU-treated and control animals (mean \pm SEM, *Lrig1*^{+/+} *n*=11, *Lrig1*^{+/-} *n*=9, *Lrig1*^{-/-} *n*=7). Two-way ANOVA: time effect (p <0.0001) and time x treatment interaction

($p < 0.0001$). Arrow indicates significant differences between all treatment groups and control arm. Tukey's multiple comparisons test $p < 0.05$. **(c)** Transverse lung sections of NTCU-treated mice stained with H&E and processed for KRT5 immunohistochemistry to identify pre-invasive airway lesions and invasive tumours. **(d)** Proportion of lower airway epithelium displaying abnormal KRT5 expression in wild-type (+/+), *Lrig1*-heterozygous (+/-) and *Lrig1*-null (-/-) mice treated with NTCU (mean \pm SEM, Kruskal-Wallis test $p = 0.038$, followed by Dunn's multiple comparisons test $*p = 0.049$, $n = 7-11$ mice per group). **(e)** KRT5-expressing lesions were categorised as flat atypia, low-grade or high-grade. Distribution of pre-invasive lesions of different grades within lower airway (mean \pm SEM). Two-way ANOVA: genotype effect ($p = 0.009$) and lesion grade effect ($p < 1 \times 10^{-6}$). The presence of flat atypia was statistically different among genotypes (Tukey's multiple comparisons test $***p = 7.7 \times 10^{-4}$, $****p = 1.7 \times 10^{-6}$). **(f)** Representative images of NTCU-induced pre-invasive lesions stained for KRT5. Scale bars represent 50 μ m. **(g)** Number of invasive tumours per mouse. Kruskal-Wallis indicated no significant differences among groups ($n = 7-11$ mice per genotype). **(h)** Size of invasive tumours in mice of different *Lrig1* genotypes (mean \pm SEM). Kruskal-Wallis test $p = 0.0002$, followed by Dunn's multiple comparisons test $**p = 0.005$, $***p = 0.0003$; *Lrig1*^{+/+} $n = 23$, *Lrig1*^{+/-} $n = 142$, *Lrig1*^{-/-} $n = 43$ invasive lesions.

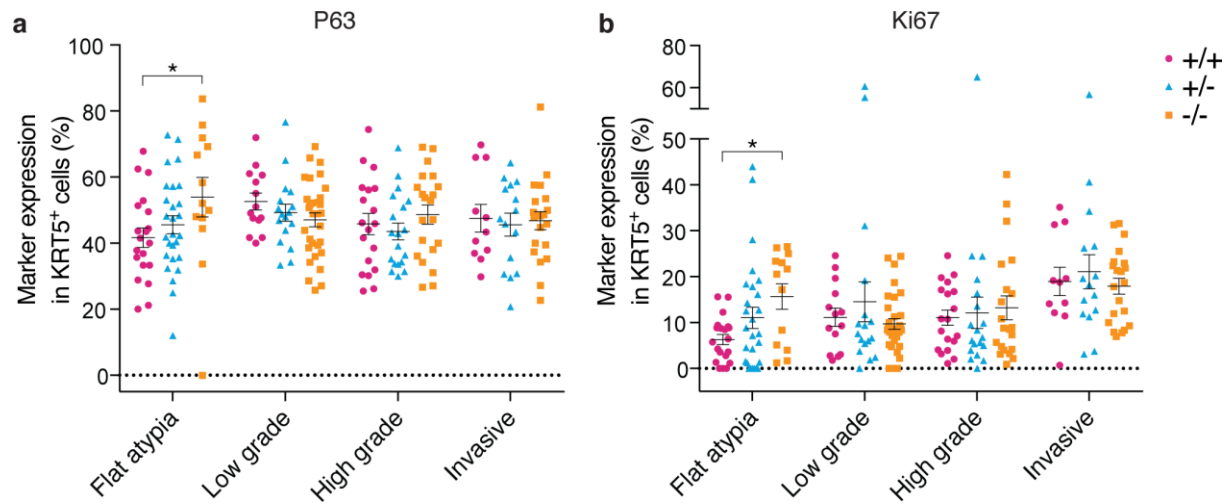


Figure 7. Characterisation of NTCU-induced lesions. **(a)** Expression of P63 in KRT5-expressing squamous airway lesions of different grades in wild-type, *Lrig1*-heterozygous and *Lrig1*-null mice (mean±SEM). **(b)** Ki67 immunoreactivity in KRT5-expressing squamous airway lesions of increasing grades in *Lrig1*^{+/+}, *Lrig1*^{+/-} and *Lrig1*^{-/-} mice (mean±SEM). For each lesion grade, the effect of *Lrig1* genotype on the fraction of KRT5⁺ cells expressing each marker was assessed. Kruskal-Wallis test $p < 0.05$, followed by Dunn's multiple comparisons test $*p < 0.05$. For both (a) and (b) $n = 11-31$ lesions/grade/genotype; KRT5⁺ cells: *Lrig1*^{+/+} $n = 6776$, *Lrig1*^{+/-} $n = 10206$, *Lrig1*^{-/-} $n = 12845$.

***Lrig1* expression identifies airway basal cells with high proliferative capacity
and restricts lung squamous cell carcinoma growth**

Laura Succony, Sandra Gómez-López, Adam Pennycuick, Ahmed S. N. Alhendi,
Derek Davies, Sarah E. Clarke, Kate H.C. Gowers, Nicholas A. Wright, Kim B.
Jensen, Sam M. Janes

Online Supplementary Material

SUPPLEMENTARY METHODS

Murine line background

The C57BL/6 *Lrig1::eGFP-IRES-CreERT²* murine line was backcrossed twice to FVB/N and maintained in a mixed C57BL/6 and FVB/N background. The choice of mouse background was influenced by strain-specific differences to both the effects of NTCU-induced carcinogenesis and the loss of *Lrig1*.

Differences in the development of pre-invasive lesions and invasive LUSC across 8 mouse strains following the application of the carcinogen NTCU for 8 months have been reported in the literature [1]. C57BL/6 mice were among the strains with lowest susceptibility to NTCU, presenting only pre-invasive lesions. FVB/N displayed intermediate susceptibility to NTCU, and have been shown to be most sensitive in other lung carcinogenesis models [2]. Under shorter term NTCU application paradigms, mice with higher NTCU susceptibility presented high mortality rates [3]. To assess development of squamous cell carcinomas with medium-period NTCU treatments, the FVB/N strain was selected with the aim of recapitulating the full spectrum of disease, without leading to excess mortality.

The selection of strain was also influenced by the strain-specific effects of loss of *Lrig1*. In an outbred mouse model, loss of *Lrig1* was shown to result in skin hyperplasia [4]. However, *Lrig1* loss in a pure FVB/N background resulted in intestinal hyperplasia so severe that mice needed to be sacrificed around postnatal day 10 [5]. This would have prevented carcinogenesis studies on this strain.

Isolation of murine tissue & cells

Animals were sacrificed by overdose of sodium pentobarbital and tissues placed either into serum free DMEM (Gibco 41966) for epithelial cell isolation, 4% paraformaldehyde (PFA)/PBS for histology or ice-cold NP40 lysis buffer (50 mM Tris-HCl pH 8.0, 150 mM NaCl, 1% IGEPAL, 1X Halt Protease and Phosphatase inhibitor cocktail (Thermo Scientific 1861281)) in preparation for immunoblotting.

Murine tracheal epithelial cells were isolated as described [6]. Additionally, the discarded tracheal scaffold was digested 30 min in 0.25% collagenase, filtered through a 40 µm cell strainer and added to the cell suspension.

Isolation of human bronchial epithelial cells

Two bronchial brushings were collected from a normal area of bronchial mucosa into ice-cold 15 mL conical tubes containing collection media (α MEM supplemented with penicillin/streptomycin and amphotericin B). Brushes were vortexed vigorously to release the cells, with the brushes remaining inside the collection tube, and then centrifuged at 300 x g for 5 min. The cells were resuspended in red cell lysis buffer (Sigma R7757) and incubated at room temperature for three minutes. Cells were resuspended in 10% FBS, 1% BSA in PBS for blocking in preparation for flow cytometry staining.

For KRT5 expression analyses, proximal airway lobectomy specimens were digested with dispase and trypsin to obtain a single cell suspension. Following cell surface staining, cells were fixed in BD CellFIX (BD Biosciences 340181) for 15 min at room temperature and permeabilised with saponin for 15 min at 4°C. Cells were then incubated with Alexa Fluor 488-conjugated anti-KRT5 antibody (Abcam ab193894) for 15 min at 4°C. Alternatively, live ITGA6⁺NGFR⁺ cells were purified, allowed to attach overnight onto collagen-coated chamber slides at 37°C and processed for immunofluorescence.

Colony forming assays

Cells were cultured at 37°C in 5% CO₂. Mitotically inactivated 3T3-J2 feeder layers were seeded at 20000 cells/cm² onto 96-well plates pre-coated with 0.05 mg/mL collagen type 1 (BD 354263) and left to adhere. The J2 media (DMEM supplemented penicillin/streptomycin (Gibco 15070) and 9% bovine serum (Gibco 26170)) was then changed to Murine Tracheal Epithelial Culture (MTEC) (for murine cells) or a 1:1 mixture of fresh FMED and J2/human bronchial epithelial cells (HBEC)-conditioned media (for human cells). MTEC consists of DMEM and F12 (Gibco 21765) in a 1:1 ratio supplemented with penicillin/streptomycin, 15 mM HEPES, 3.6 mM Na₂CO₃, 10 µg/mL insulin (Sigma I6634), 5 µg/mL transferrin (Sigma T1147), 0.1 µg/mL cholera toxin (Sigma C3012), 25 ng/mL EGF (BD 354001), 30 µg/mL bovine pituitary extract

(ThermoFisher 13028014), 5% foetal bovine serum (FBS, Gibco 10270) and freshly added 0.01 μ M retinoic acid (Sigma R2625). FMED consists of DMEM and F12 in a 3:1 ratio supplemented 7.5% FBS, penicillin/streptomycin, 5 μ M Y-27632 (ROCK inhibitor, Cambridge Bioscience Y1000), 25 ng/mL hydrocortisone (Sigma HO888), 0.125 ng/mL human recombinant EGF (Sino Biological 10605), 5 μ g/mL insulin, 0.1 nM cholera toxin, 250 ng/mL amphotericin B (Fisher Scientific 10746254) and 10 μ g/mL gentamicin (Gibco 15710). Single basal epithelial cells were sorted directly into each well. MTEC or FMED/conditioned media was changed 3 times a week. Human and murine cultures were fixed with 4% PFA at day 10 or 14, respectively, and stained with crystal violet for counting.

Tracheosphere assay

Flow cytometry-sorted murine basal epithelial cells were plated at 1250 cells/well in Matrigel (BD Biosciences 354230) and cultured in MTEC media. After 7 days, the media was changed to differentiation media, which is based on MTEC, except that contains a lower concentration of EGF (5 ng/mL) and cholera toxin (0.025 μ g/mL), and includes 1 mg/mL bovine serum albumin (BSA). At day 14, spheres were counted, and imaged.

***LRIG1* knockdown in human bronchial epithelial cells**

Lentiviral vectors (pGIPZ) expressing green fluorescent protein (GFP) along with an shRNA against *LRIG1* (Open Biosystems V2LHS_229246) or a control non-silencing construct were used. Recombinant lentiviruses were produced by co-transfection of 293T cells with each pGIPZ vector together with packaging plasmids pCMVR8.74 and pMD2.G (Addgene plasmids #22036 and #12259) using the DNA transfection reagent jetPEI (Source Bioscience UK Ltd). Lentiviruses were concentrated by ultracentrifugation and titrated in 293T cells using GFP expression as readout. Human bronchial epithelial cells were expanded on 3T3-J2 feeder layers in FMED, as previously reported [7], and transduced at an multiplicity of infection (MOI) of 3 in the presence of 4 μ g/mL polybrene (Sigma).

XTT proliferation assay

7,500 cells/well were plated into 96-well plates in complete BEGM (Lonza CC-2540B). Cells were left to adhere overnight, the media was then changed and XTT

(Applichem A8088) added at each time point according to the manufacturers' instructions. After 4h incubation, the absorbance was measured using a Titertec Multiscan MCC/340 plate reader (Labsystems, Turku, Finland) at wavelengths of 490 and 630 nm. The 630 nm measurement was subtracted from the 490 nm to obtain the absorbance reading. Percentage change was expressed as a proportion of the initial reading.

Immunoblotting

Dissected cerebella from 6-8-week-old mice were lysed in NP40 buffer. Human bronchial epithelial cells were lysed in RIPA buffer (Sigma R0278). Protein concentration of cleared supernatants was determined by BCA assays (Pierce Thermo Scientific 23225). Equivalent amounts of protein were resolved in 4-12% Bis-Tris gels and transferred onto nitrocellulose membranes. Membranes were blocked and incubated with primary antibodies (Supplementary Table 2) in 5% BSA/TBST overnight at 4°C. HRP-conjugated secondary antibodies were added and immunoblots analysed using Luminata Western HRP Chemiluminescence Reagent (Millipore WBLUR0500) on the ImageQuant LAS 4000 system (GE Healthcare).

Histology and immunofluorescence

Paraffin-embedded samples were sectioned at 4 µm. Heat-induced antigen retrieval was performed in 10 mM Sodium Citrate pH 6.0 in a microwave oven. This step was omitted when staining for GFP, in which case samples were permeabilised with 0.2% Triton X/PBS for 10 min before blocking. Fresh-frozen OCT-embedded human samples were sectioned, left to dry, fixed 10 min in 4%PFA and washed in PBS before incubating with blocking solution. For whole-mount immunofluorescence of mouse airways, the airways of the left lung lobe were microdissected under a stereomicroscope (Leica S9i) to expose the epithelium prior to antibody staining. Cells on collagen-coated chambers slides were fixed with 4%PFA for 10 min and washed with PBS before immunostaining. Primary antibodies were: GFP (Abcam ab13970), KRT5 (Abcam ab53121, BioLegend 905501 and 905901), human LRIG1 (R&D MAB7498), acetylated-tubulin (Sigma T6793), anti-SCGB1A1 (kind gift from Barry Stripp and Santa Cruz sc-9772), p63 (Abcam ab53039 and ab735, Cell Signaling Technology 13109), and Ki67 (eBioscience 14-5698). Secondary antibodies were conjugated to Alexa Fluor dyes (Life Technologies or Jackson

ImmunoResearch) or streptavidin-HRP (DAKO). Fluorescently-labelled sections were mounted in Immu-Mount (Thermo Scientific 9990402) or Fluoromount G (SouthernBiotech 01000-01). Whole-mount preparations were mounted in RapiClear 1.52 (SunJin Lab RC152001). Confocal images were obtained using a Zeiss LSM700 or an LSM880; epifluorescence images were acquired on a Leica DMI8 microscope. Image analyses were done using Fiji.

NTCU model analysis

Lungs from NTCU-treated and control groups were sectioned transversely until the trachea and main bronchi were visualised. Two 4 μm sections were cut, followed by two further sections 200 μm from the first. The first of the two sections were stained with haematoxylin and eosin (H&E) and the second immunostained for KRT5. Stained sections were imaged on a Nanozoomer (Hamamatsu). The NDP.view 2 software (Hamamatsu) was used to trace around the outline of the entire visible bronchial tree beyond the cartilage containing trachea and the beginning of right and left main bronchi (Fig. 5c). Any KRT5 staining distal to the origin of the right and left main bronchi was also drawn around. The KRT5 abnormal areas were categorised into each type of lesion: high-grade, low-grade or flat atypia. The percentage of bronchial tree affected by all pre-invasive lesions, together with the percentage of bronchial tree affected by each grade of lesion was calculated. A mean across two sections of bronchial tree was determined. Tumour size was determined by drawing around the circumference of each invasive area within a section. Lesions were counted as discrete if greater than 200 μm apart. Lesions across the two sections, 200 μm apart were included.

Analysis of the Human Lung Cell Atlas scRNAseq dataset

A scRNAseq dataset including ~75000 cells from three lung locations (alveolar, bronchiole and bronchi) was obtained from the Human Lung Cell Atlas (<https://hlca.ds.czbiohub.org/>) [8]. Using the cell type annotations provided in metadata, the single-cell RNA data from droplet 10X Chromium (10X) was filtered for normal human basal cells from epithelial tissue collected from the bronchi. The number of basal cells after filtering was 367. Genes enriched in each basal cell cluster have been described by Travaglini and colleagues [8]. The proliferative signature was defined by the expression of *PBK*, *BIRC5*, *MKI67*, *UBE2C*, *TOP2A*,

TK1, *AURKB*, *CDKN3*, *CENPF*, *CDK1* and *ZWINT*. Analyses including QC metric, normalisation, scaling and gene expression were performed using the R package Seurat v 4.0 [9]. Principal component analysis (PCA) dimensionality reduction was performed using the highly variable genes as input. The PCs were used to calculate t-distributed stochastic neighbour embedding (t-SNE). The number of PCs used for t-SNE was dataset-dependent and estimated by the elbow of a PCA scree plot. The average gene expression of selected genes and cell counts were calculated in each basal annotation after separating them based on *LRIG1* gene expression. The correlation between *LRIG1* and *MKI67* expressions in proliferating basal cells was performed using Pearson correlation in R software.

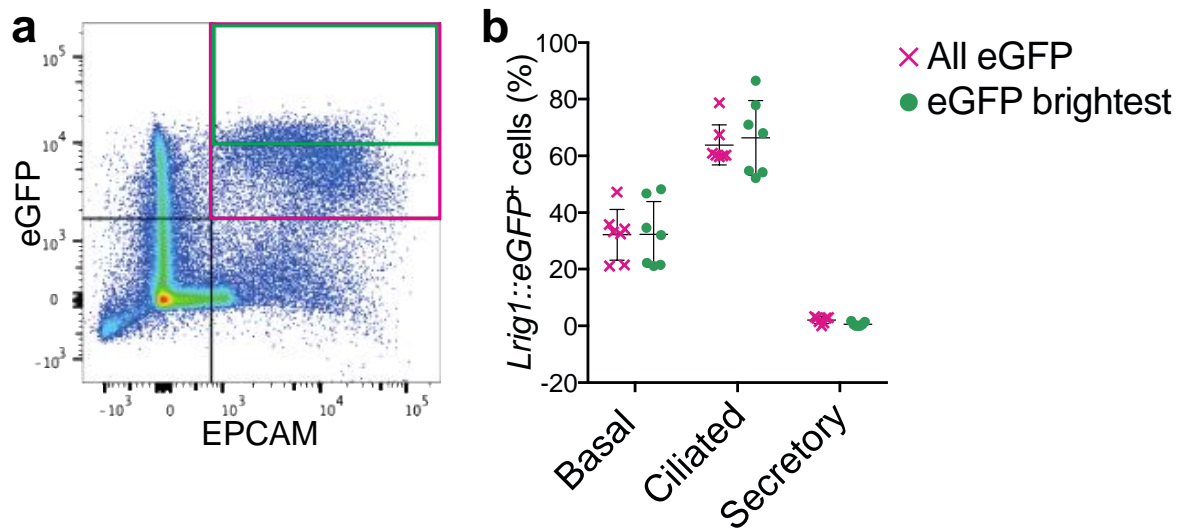
Supplementary Table 1. Flow cytometry reagents

Reagent	Supplier	Code
Anti-mouse CD31	BioLegend	102407 and 102417
Anti-mouse CD45	BioLegend	103105
Anti-mouse EpCAM	BD Biosciences	563134
Isolectin GS-IB4 biotin conjugate	Invitrogen	I21414
Qdot 605 streptavidin conjugate	Invitrogen	Q10101MP
Anti-mouse CD24	BioLegend	101821
Anti-mouse SSEA1	eBioscience	46-8813-41
Anti-CD49f (ITGA6)	eBioscience	17-0495-80
Anti-human CD31	BioLegend	303106 and 303124
Anti-human CD45	BioLegend	368510 and 304032
Anti-human LRIG1	R&D Systems	FAB7498P
Anti-human NGFR	BioLegend	345110

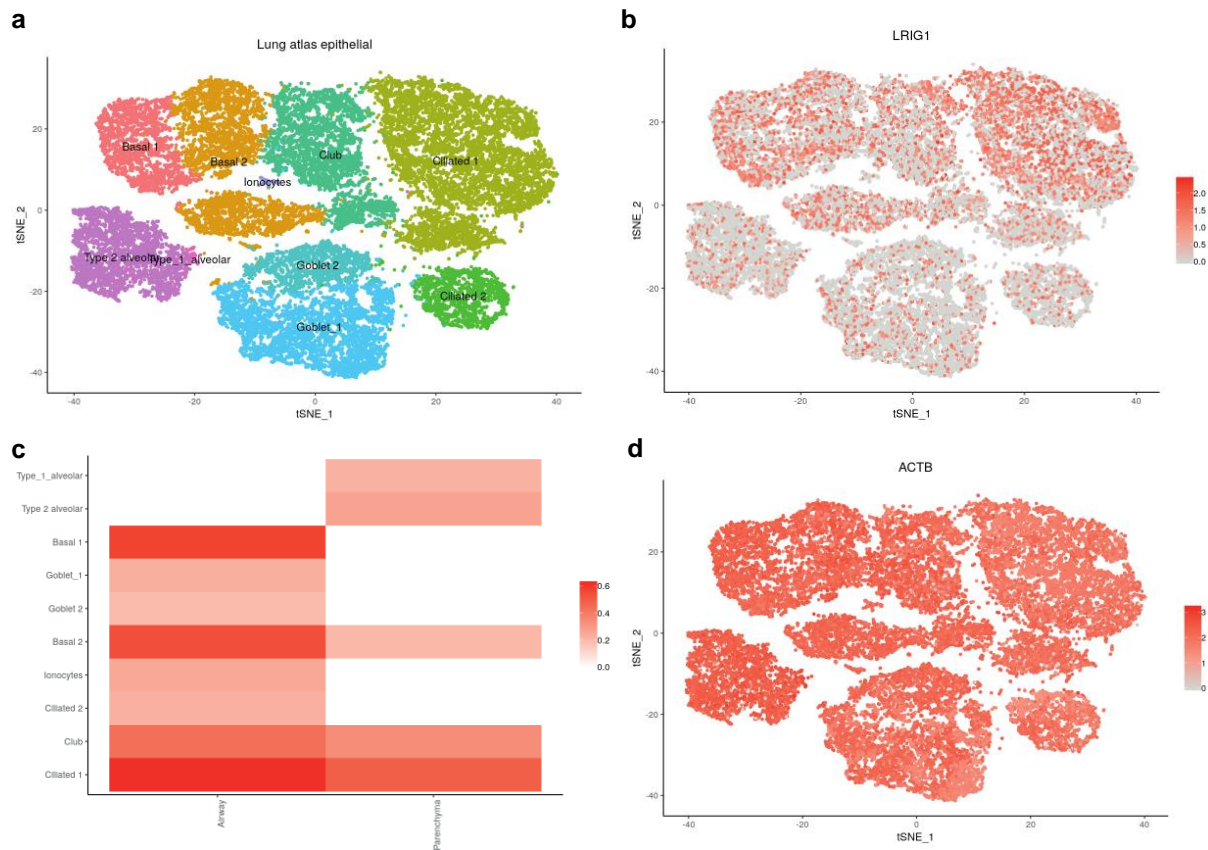
Supplementary Table 2. Antibodies for immunoblotting

Antigen	Host	Supplier	Code	Concentration
mouse LRIG1	Rabbit	Abcam	Ab36707	1 µg/ml
human LRIG1	Rabbit	Cell Signaling Technology	#12752	1:1000
α-tubulin	Rabbit	Cell Signaling Technology	#9099	1:1000
EGFR	Rabbit	Cell Signaling Technology	#4267	1:1000
phospho-EGFR	Rabbit	Cell Signaling Technology	#2234	1:1000
ERK 1/2	Rabbit	Cell Signaling Technology	#9102	1:1000
phospho-ERK 1/2	Rabbit	Cell Signaling Technology	#9101	1:1000

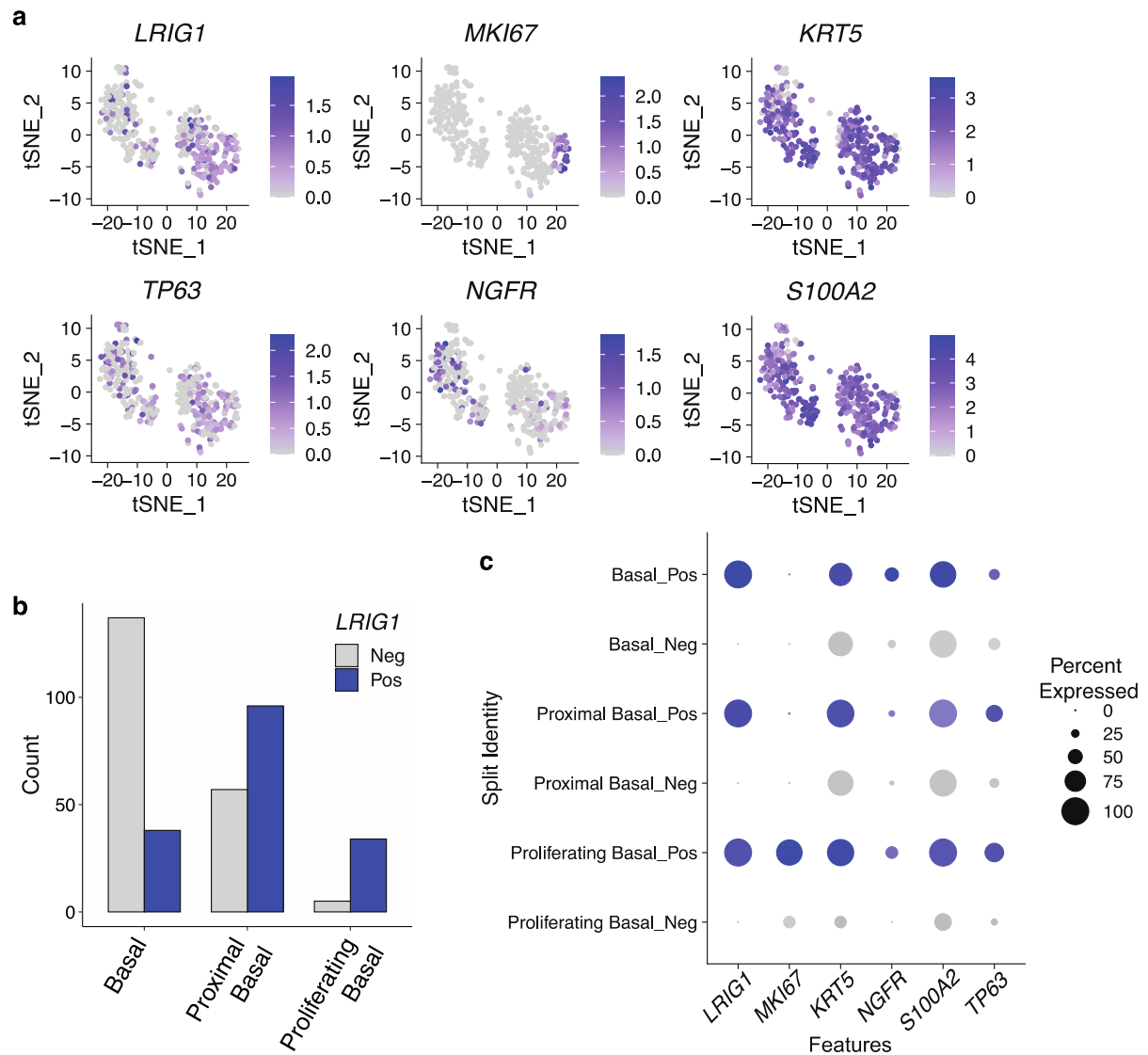
SUPPLEMENTARY FIGURES



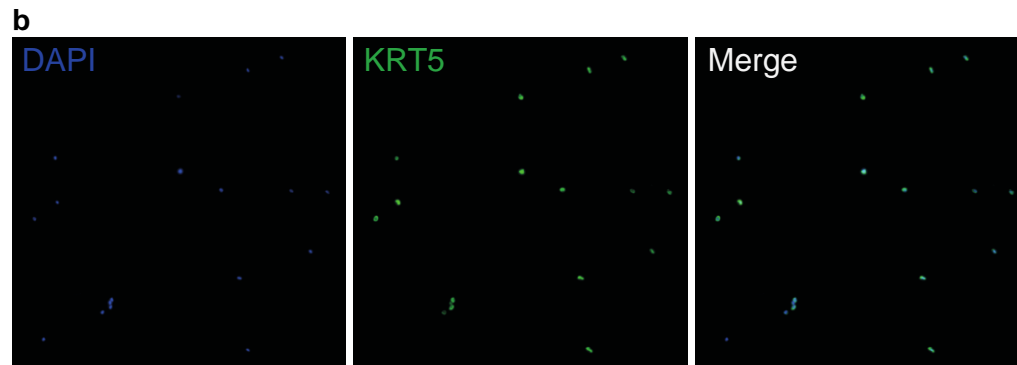
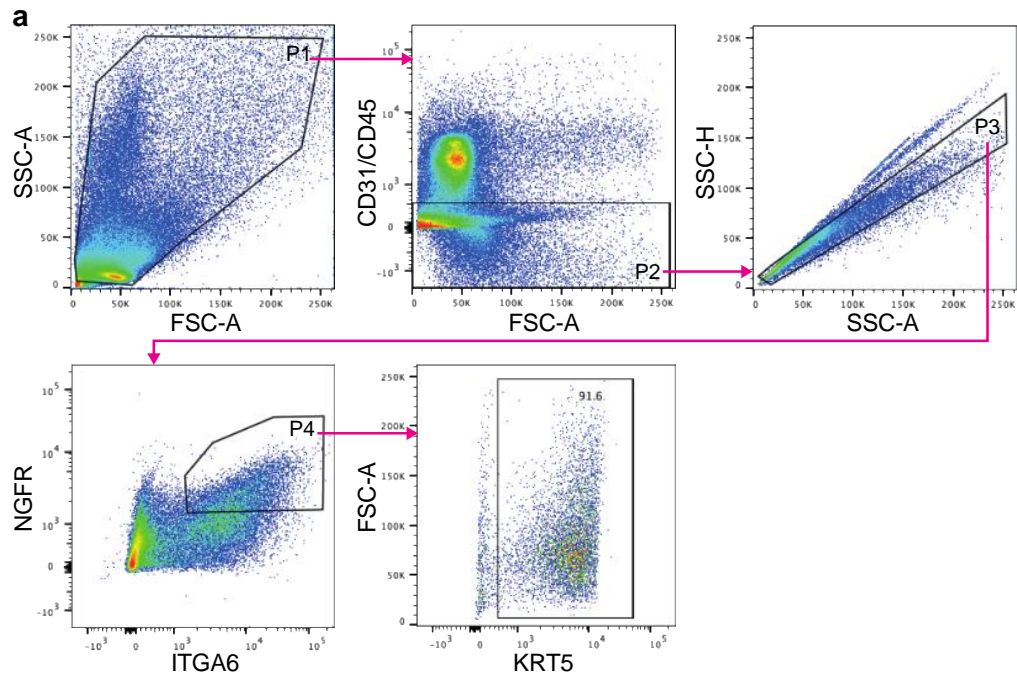
Supplementary Figure 1. Expression of *Lrig1::eGFP* in the murine upper airways. Immunophenotypic characterisation of tracheal epithelial cells expressing *Lrig1::eGFP* by flow cytometry. Live tracheal epithelial cells were identified by negative selection of cells expressing CD31, CD45 and DAPI, followed by positive selection of EPCAM⁺eGFP⁺ cells. **(a)** Flow cytometry plot showing total EPCAM⁺eGFP⁺ cells (magenta box) and the brightest eGFP⁺ fraction (green box). **(b)** The distribution of GSI-B4⁺ basal cells, ciliated CD24⁺ cells and SSEA1⁺ secretory cells were compared in the EPCAM⁺eGFP⁺ populations indicated in a (mean±SEM, *n*=7).



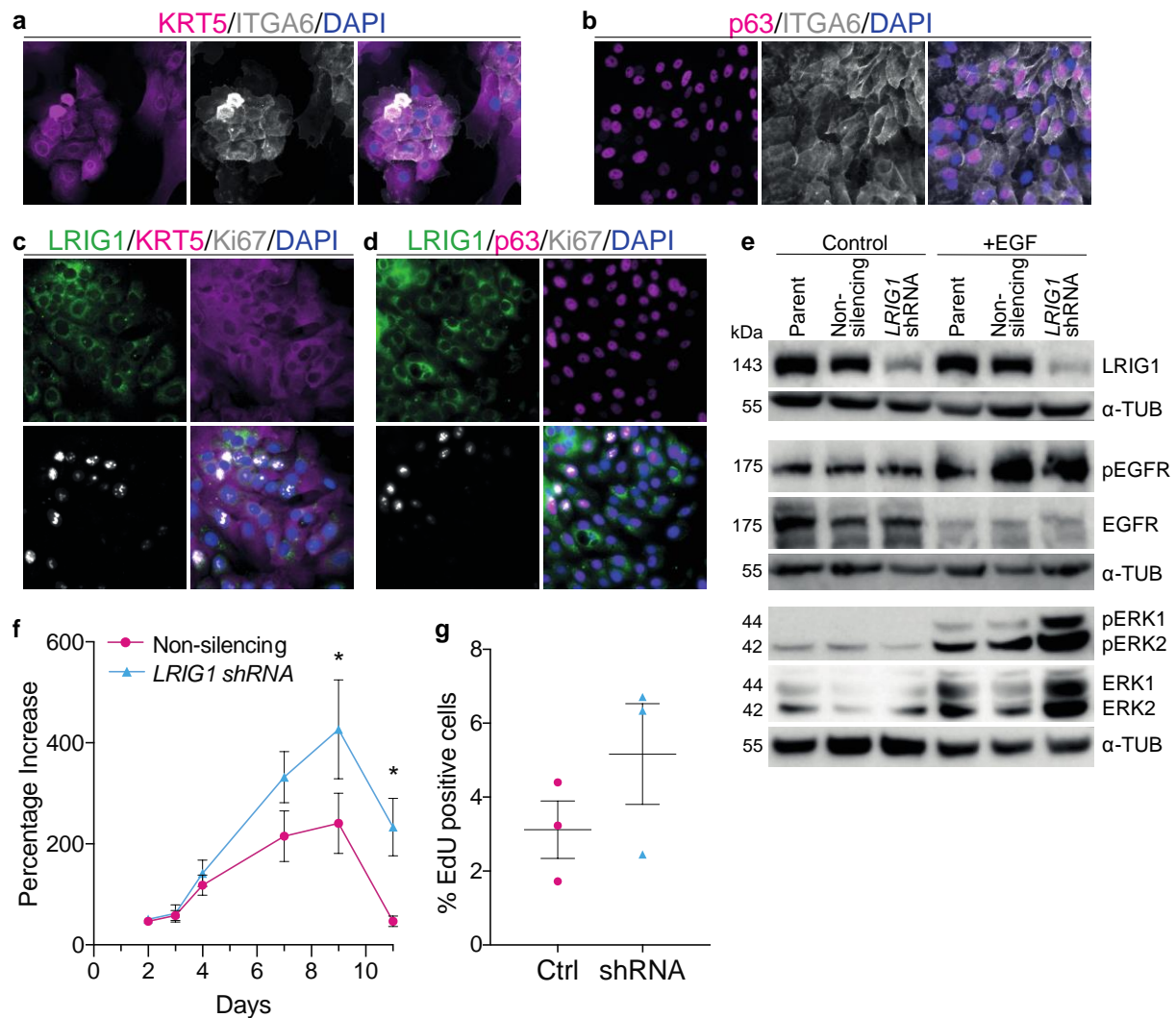
Supplementary Figure 2. Expression of *LRIG1* in the human adult airway epithelium. **(a)** Epithelial cell clusters present in the human airways. **(b & c)** Expression of *LRIG1* within the different human airway epithelial cell populations as assessed by single-cell RNA sequencing of 36 931 single cells from the human airways and lung parenchyma [10]. **(d)** Expression levels of the housekeeping gene *ACTB* are shown for comparison. Plots were downloaded from the www.lungcellatlas.org web portal.



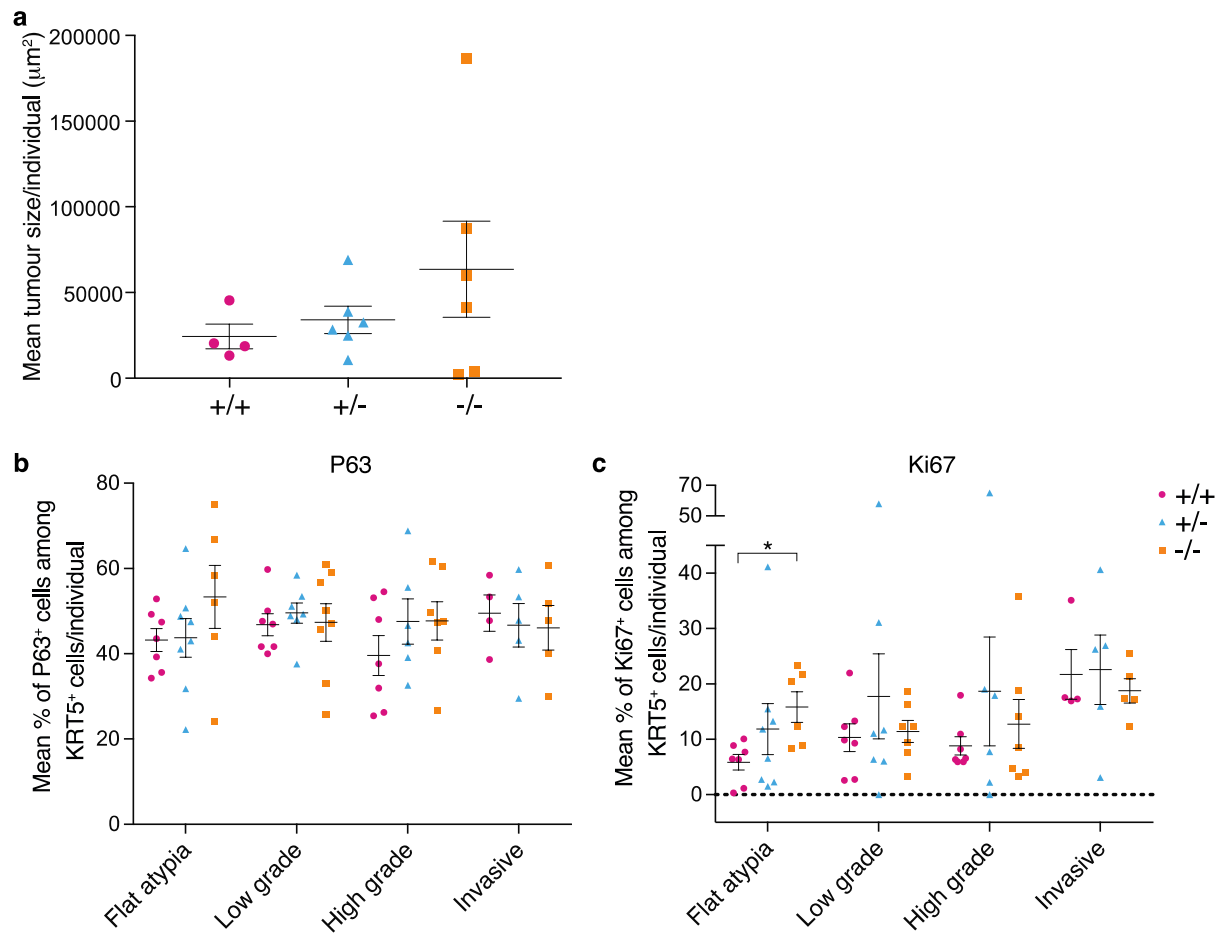
Supplementary Figure 3. Expression of *LRIG1* in bronchial basal cell clusters from the scRNAseq Human Lung Cell Atlas dataset. Normal human basal cells from bronchial epithelial tissue ($n=367$) were used to explore differences between the *LRIG1*⁺ and *LRIG1*⁻ subpopulations. **(a)** Feature plot displaying gene expression of *LRIG1* and selected marker genes in bronchial basal cells. **(b)** Count of cells with or without *LRIG1* expression in each basal cell cluster. **(c)** Dot plot depicting gene expression levels and percentage of cells expressing the indicated genes in *LRIG1* positive (Pos) or negative (Neg) basal cells.



Supplementary Figure 4. Characterisation of flow-cytometry purified ITGA6⁺NGFR⁺ human bronchial epithelial cells. **(a)** Following exclusion of debris, a cell population was selected (P1), from which both haematopoietic (CD45⁺) and endothelial (CD31⁺) cells were removed (P2). Single cells (P3) co-expressing ITGA6 and NGFR were then selected (P4). Within this double positive population, the fraction of cells expressing the basal cell marker KRT5 was assessed using intracellular staining. 85.6%±2.9 (mean±SEM, *n*=3 donors) of ITGA6⁺NGFR⁺ human bronchial epithelial cells were KRT5⁺. **(b)** Immunofluorescence staining for KRT5 in flow-cytometry purified ITGA6⁺NGFR⁺ human bronchial epithelial cells.



Supplementary Figure 5. LRIG1 is expressed in primary human bronchial epithelial cells (HBECs) *in vitro*. **(a, b)** Primary HBECs express the basal cell markers KRT5, ITGA6 and p63 *in vitro*. **(c,d)** Immunofluorescence staining for LRIG1, the basal cell markers KRT5 and p63, and the proliferation marker Ki67 in cultured HBECs. HBECs were transduced with lentivirus expressing either an shRNA against *LRIG1* or a control non-silencing construct. **(e)** Modified HBECs were starved for 16h and stimulated with or without 10 ng/mL EGF for 30 min. Immunoblot confirming successful *LRIG1* knockdown in cells carrying the *LRIG1* shRNA construct. *LRIG1* knockdown results in enhanced EGFR signalling activation. **(f)** XTT viability assays show enhanced expansion rate in *LRIG1* knockdown HBEC cultures when compared to controls (mean \pm SEM, $n=4$ donors). Two-way ANOVA: treatment effect ($p=0.0016$) and time effect ($p<0.0001$). *Sidak's multiple comparison test $p<0.03$. **(g)** EdU incorporation assay following *LRIG1* knockdown in HBECs (mean \pm SEM, $n=3$ donors). Ratio paired t -test ($p=0.0599$).



Supplementary Figure 6. Analysis of NTCU-induced pre-invasive lung lesions and tumours in individual mice of different *Lrig1* genotypes. **(a)** Average size of invasive LUSC tumours in individual wild-type (+/+), *Lrig1*-heterozygous (+/-) and *Lrig1*-null (-/-) mice treated with NTCU. Mean \pm SEM for individuals of the same genotype is also shown. The proportion of KRT5⁺ cells expressing **(b)** P63 and **(c)** Ki67 in lesions of distinct grades was quantified. Dot plots represent average ratios in individual mice. For each lesion type, mean \pm SEM of values from mice of the same genotype is also shown. *Kruskal-Wallis test $p=0.037$, followed by Dunn's multiple comparisons test $p=0.036$.

SUPPLEMENTARY REFERENCES

1. Wang Y, Zhang Z, Yan Y, Lemon WJ, LaRegina M, Morrison C, Lubet R, You M. A chemically induced model for squamous cell carcinoma of the lung in mice: histopathology and strain susceptibility. *Cancer Res* 2004; 64(5): 1647-1654.
2. Stathopoulos GT, Sherrill TP, Cheng DS, Scoggins RM, Han W, Polosukhin VV, Connelly L, Yull FE, Fingleton B, Blackwell TS. Epithelial NF-kappaB activation promotes urethane-induced lung carcinogenesis. *Proc Natl Acad Sci U S A* 2007; 104(47): 18514-18519.
3. Tago Y, Yamano S, Wei M, Kakehashi A, Kitano M, Fujioka M, Ishii N, Wanibuchi H. Novel medium-term carcinogenesis model for lung squamous cell carcinoma induced by N-nitroso-tris-chloroethylurea in mice. *Cancer Sci* 2013; 104(12): 1560-1566.
4. Suzuki Y, Miura H, Tanemura A, Kobayashi K, Kondoh G, Sano S, Ozawa K, Inui S, Nakata A, Takagi T, Tohyama M, Yoshikawa K, Itami S. Targeted disruption of LIG-1 gene results in psoriasiform epidermal hyperplasia. *FEBS letters* 2002; 521(1-3): 67-71.
5. Wong VW, Stange DE, Page ME, Buczacki S, Wabik A, Itami S, van de Wetering M, Poulsom R, Wright NA, Trotter MW, Watt FM, Winton DJ, Clevers H, Jensen KB. Lrig1 controls intestinal stem-cell homeostasis by negative regulation of ErbB signalling. *Nat Cell Biol* 2012; 14(4): 401-408.
6. Hegab AE, Ha VL, Attiga YS, Nickerson DW, Gomperts BN. Isolation of basal cells and submucosal gland duct cells from mouse trachea. *J Vis Exp* 2012(67): e3731.
7. Butler CR, Hynds RE, Gowers KH, Lee Ddo H, Brown JM, Crowley C, Teixeira VH, Smith CM, Urbani L, Hamilton NJ, Thakrar RM, Booth HL, Birchall MA, De Coppi P, Giangreco A, O'Callaghan C, Janes SM. Rapid Expansion of Human Epithelial Stem Cells Suitable for Airway Tissue Engineering. *Am J Respir Crit Care Med* 2016; 194(2): 156-168.
8. Travaglini KJ, Nabhan AN, Penland L, Sinha R, Gillich A, Sit RV, Chang S, Conley SD, Mori Y, Seita J, Berry GJ, Shrager JB, Metzger RJ, Kuo CS, Neff N, Weissman IL, Quake SR, Krasnow MA. A molecular cell atlas of the human lung from single-cell RNA sequencing. *Nature* 2020; 587(7835): 619-625.
9. Butler A, Hoffman P, Smibert P, Papalexi E, Satija R. Integrating single-cell transcriptomic data across different conditions, technologies, and species. *Nature biotechnology* 2018; 36(5): 411-420.
10. Vieira Braga FA, Kar G, Berg M, Carpaij OA, Polanski K, Simon LM, Brouwer S, Gomes T, Hesse L, Jiang J, Fasouli ES, Efremova M, Vento-Tormo R, Talavera-Lopez C, Jonker MR, Affleck K, Palit S, Strzelecka PM, Firth HV, Mahbubani KT, Cvejic A, Meyer KB, Saeb-Parsy K, Luinge M, Brandsma CA, Timens W, Angelidis I, Strunz M, Koppelman GH, van Oosterhout AJ, Schiller HB, Theis FJ, van den Berge M, Nawijn MC, Teichmann SA. A cellular census of human lungs identifies novel cell states in health and in asthma. *Nat Med* 2019; 25(7): 1153-1163.